

# NAVAL POSTGRADUATE SCHOOL MONTEREY, CALIFORNIA



## THESIS

**CONSTRUCTION AND PERFORMANCE  
MEASUREMENT OF A PORTABLE  
THERMOACOUSTIC REFRIGERATOR  
DEMONSTRATION APPARATUS**

by

Todd J. Berhow

December, 1994

Thesis Advisor:

Thomas J. Hofler

Approved for public release; distribution is unlimited.

19950411 056

DTIC QUALITY INSPECTED 5

REPORT DOCUMENTATION PAGE			Form Approved OMB No. 0704-0188	
Public reporting burden for this collection of information is estimated to average 1 hour per response, including the time for reviewing instruction, searching existing data sources, gathering and maintaining the data needed, and completing and reviewing the collection of information. Send comments regarding this burden estimate or any other aspect of this collection of information, including suggestions for reducing this burden, to Washington Headquarters Services, Directorate for Information Operations and Reports, 1215 Jefferson Davis Highway, Suite 1204, Arlington, VA 22202-4302, and to the Office of Management and Budget, Paperwork Reduction Project (0704-0188) Washington DC 20503.				
1. AGENCY USE ONLY (Leave blank)		2. REPORT DATE December 1994		3. REPORT TYPE AND DATES COVERED Master's Thesis
4. TITLE AND SUBTITLE CONSTRUCTION AND PERFORMANCE MEASUREMENT OF A PORTABLE THERMOACOUSTIC REFRIGERATOR DEMONSTRATION APPARATUS			5. FUNDING NUMBERS	
6. AUTHOR(S) Lieutenant Todd J. Berhow, U.S. Navy				
7. PERFORMING ORGANIZATION NAME(S) AND ADDRESS(ES) Naval Postgraduate School Monterey CA 93943-5000			8. PERFORMING ORGANIZATION REPORT NUMBER	
9. SPONSORING/MONITORING AGENCY NAME(S) AND ADDRESS(ES)			10. SPONSORING/MONITORING AGENCY REPORT NUMBER	
11. SUPPLEMENTARY NOTES The views expressed in this thesis are those of the author and do not reflect the official policy or position of the Department of Defense or the U.S. Government.				
12a. DISTRIBUTION/AVAILABILITY STATEMENT Approved for public release; distribution is unlimited.			12b. DISTRIBUTION CODE	
13. ABSTRACT (maximum 200 words) This thesis documents the construction and performance measurement of a portable thermoacoustic refrigerator demonstration apparatus. The objective of the portable refrigerator is to graphically display, as a demonstration during lectures, a substantial thermoacoustic cooling power. Within minutes of start up, the apparatus develops frost on a small metal portion of the device. The refrigerator is small and compact and fits into a portable carrying case along with all ancillary equipment. The construction of the device had been started in a previous thesis project. This thesis describes the remaining construction steps required to complete the refrigerator and the subsequent performance evaluation of the unit in laboratory test trials.				
14. SUBJECT TERMS Portable Thermoacoustic Demonstration Refrigerator			15. NUMBER OF PAGES 96	
			16. PRICE CODE	
17. SECURITY CLASSIFICATION OF REPORT Unclassified	18. SECURITY CLASSIFICATION OF THIS PAGE Unclassified	19. SECURITY CLASSIFICATION OF ABSTRACT Unclassified	20. LIMITATION OF ABSTRACT UL	

NSN 7540-01-280-5500

Standard Form 298 (Rev. 2-89)

Prescribed by ANSI Std. Z39-18 298-102



Approved for public release; distribution is unlimited.

Construction and Performance Measurement of a Portable Thermoacoustic  
Refrigerator Demonstration Apparatus

by

Todd J. Berhow  
Lieutenant, United States Navy  
B.S., North Dakota State University, 1986

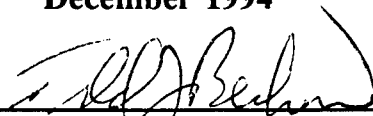
Submitted in partial fulfillment  
of the requirements for the degree of

**MASTER OF SCIENCE IN APPLIED PHYSICS**

from the

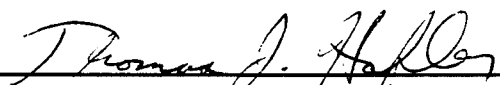
**NAVAL POSTGRADUATE SCHOOL  
December 1994**

Author:



Todd J. Berhow

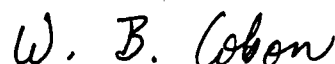
Approved by:



Thomas J. Hofler, Thesis Advisor



Anthony A. Atchley, Co-Advisor



William B. Colson, Chairman  
Department of Physics

Accession For	
NTIS	CRA&I <input checked="" type="checkbox"/>
DTIC	TAB <input type="checkbox"/>
Unannounced <input type="checkbox"/>	
Justification _____	
By _____	
Distribution / _____	
Availability Codes	
Dist	Avail and/or Special
A-1	



## ABSTRACT

This thesis documents the construction and performance measurement of a portable thermoacoustic refrigerator demonstration apparatus. The objective of the portable refrigerator is to graphically display, as a demonstration during lectures, a substantial thermoacoustic cooling power. Within minutes of start up, the apparatus develops frost on a small metal portion of the device. The refrigerator is small and compact and fits into a portable carrying case along with all ancillary equipment. The construction of the device had been started in a previous thesis project. This thesis describes the remaining construction steps required to complete the refrigerator and the subsequent performance evaluation of the unit in laboratory test trials.



## TABLE OF CONTENTS

<b>I.</b>	<b>INTRODUCTION .....</b>	<b>1</b>
<b>A.</b>	<b>THERMOACOUSTIC REFRIGERATION .....</b>	<b>1</b>
<b>B.</b>	<b>HISTORY OF THERMOACOUSTIC REFRIGERATORS.....</b>	<b>4</b>
1.	The Hofler Refrigerator.....	4
2.	The Space Thermoacoustic Refrigerator (S.T.A.R.).....	4
3.	An Early Demonstration Refrigerator.....	4
4.	The Brooks Demonstration Refrigerator.....	4
<b>II.</b>	<b>DEMONSTRATION REFRIGERATOR.....</b>	<b>9</b>
<b>A.</b>	<b>OBJECTIVES OF THE NEW REFRIGERATOR .....</b>	<b>9</b>
1.	Cold/Frosted Metal Part .....	9
2.	Compact/Portable Demonstration Model .....	9
3.	Air Cooled Operation .....	9
<b>B.</b>	<b>BASIC DESIGN .....</b>	<b>10</b>
1.	Mode/Adeff Acoustic Driver .....	10
2.	Brooks Resonator .....	12
a.	<i>Resonator Parameters</i> .....	12
b.	<i>Optimized Parameters</i> .....	13
c.	<i>Performance Predicted by Optimization</i> .....	14
d.	<i>Finned Heat Exchangers with Crossbars</i> .....	14
3.	Air Duct and Fan .....	17
<b>III.</b>	<b>MEASUREMENTS .....</b>	<b>21</b>
<b>A.</b>	<b>FIRST REFRIGERATION TESTS .....</b>	<b>21</b>
<b>B.</b>	<b>ELECTRICAL IMPEDANCE MEASUREMENTS .....</b>	<b>24</b>
1.	Uninsulated Resonator at Different Temperatures .....	24
2.	Insulated Resonator at Different Temperatures .....	28
<b>C.</b>	<b>TEMPERATURE AS A FUNCTION OF TIME .....</b>	<b>32</b>
1.	Measurement Conditions .....	32
2.	Uninsulated and Insulated Resonator Measurements.....	33
3.	Cold Heat Capacity Gives Heat Power Information.....	37
4.	Driver and Heat Exchanger Temperature with Fast/Slow Fans .....	40
<b>D.</b>	<b>STEADY COOLING POWER WITH ELECTRIC HEAT LOADS ....</b>	<b>41</b>
1.	Thermal and Acoustic Power Measurement Procedures .....	41
2.	Comparing Steady State and Time Dependent Cooling Power Data .....	42
3.	Computing Coefficient of Performance and Efficiencies.....	44
<b>IV.</b>	<b>PACKAGING .....</b>	<b>51</b>
<b>A.</b>	<b>COMPACT/EFFICIENT ELECTRIC POWER AMPLIFIER.....</b>	<b>51</b>
1.	Basic Circuit .....	51
2.	Inductor used with Circuit .....	51
3.	Square Wave Switching Circuit .....	52
4.	Efficiency with Load Resistor .....	55



B. ANCILLARY EQUIPMENT .....	55
V. CONCLUSION .....	57
A. SUCCESSFUL DEMONSTRATION.....	57
B. POWER DENSITY IMPROVEMENT .....	57
C. THERMOACOUSTIC EFFICIENCY IMPROVEMENT .....	58
D. PROBLEMS AND SUGGESTIONS .....	58
APPENDIX. CONSTRUCTION DRAWINGS .....	61
LIST OF REFERENCES .....	79
INITIAL DISTRIBUTION LIST .....	81

## LIST OF FIGURES

1. Thermoacoustic Stack .....	3
2. Space Thermoacoustic Refrigerator (S.T.A.R.) .....	6
3. Original Lucite "Demo-Frig" .....	7
4. Demonstration Refrigerator Section .....	11
5. Cold Heat Exchanger .....	15
6. Hot Heat Exchanger .....	16
7. Schematic Airflow for Shroud .....	18
8. Frosted Cold Heat Exchanger .....	23
9. Electric Impedance at Cold Operating Temperature (Uninsulated) .....	26
10. Electric Impedance at Warm Operating Temperature (Uninsulated) .....	27
11. Acoustic Resonant Frequency versus Temperature .....	29
12. Electric Impedance at Cold Operating Temperature (Insulated) .....	30
13. Electric Impedance at Warm Operating Temperature (Insulated) .....	31
14. Time Dependent Refrigerator Performance (Uninsulated) .....	34
15. Time Dependent Refrigerator Performance (Insulated) .....	36
16. Steady State and Time Dependent Cooling Power Data .....	43
17. Plots of Total Cooling Power verses Temperature Span and COP .....	47
18. Acoustic Driver Circuit Schematic .....	54
19. Cowling Cylinder (drawing #1) .....	62
20. Cowling Cylinder (drawing #2) .....	63
21. Cowling Cylinder (drawing #3) .....	64
22. Cowling Cylinder (drawing #4) .....	65
23. Cowling Cylinder (drawing #5) .....	66
24. Cowling Cylinder (drawing #6) .....	67
25. Cowling Lid (drawing #1) .....	68
26. Cowling Lid (drawing #2) .....	69
27. Cowling Legs .....	70
28. Cowling Bracket .....	71
29. Cowling Base (drawing #1) .....	72
30. Cowling Base (drawing #2) .....	73
31. Resonator Flange Standoff .....	74
32. Valve Stem Extension .....	75
33. Resonator Shield .....	76
34. Air Deflector .....	77
35. Air Shield Grip .....	78



## LIST OF EQUIPMENT

1. TECHRON 5507 Power Supply Amplifier, Crown International Corporation, Elkhart, Indiana, Serial Number: 238314.
2. Hewlett Packard 4192A LF Impedance Analyzer, Hewlett Packard Company, Marysville, Washington, Serial Number: 2514J03706.
3. Hewlett Packard 3478A Multimeter, Hewlett Packard Company, Marysville, Washington, Serial Number: 2911A59877.
4. Hewlett Packard 3314A Function Generator, Hewlett Packard Company, Marysville, Washington, Serial Number: 2836A13113.
5. KEITHLEY 740 System Scanning Thermometer, Keithley Instrumentation Incorporated, Cleveland, Ohio, Serial Number: 496518.
6. Hewlett Packard 3457A Digital Multimeter, Hewlett Packard Company, Marysville, Washington, Serial Number: 3114A12968.
7. Kikusui Par 160A Regulated D. C. Power Supply, Kikusui International Corporation, Torrance, California, Serial Number: 29010421.



## ACKNOWLEDGMENT

The author would like to sincerely thank Dr. Thomas J. Hofler for the many long hours spent teaching and proofing to make this thesis possible. His expertise and devotion to the subject are an inspiration to all who have the pleasure to work with him. Truly, it was a great honor to have learned thermoacoustics from such a distinguished scholar.

In addition, the author would like to thank Mr. Jay Adeff for his assistance in all Computer Aided Design and Drafting (CADD) requirements as well as all photographic and computer software assistance. His engineering experience and sound judgment proved to be priceless.

I would also thank Dr. Anthony Atchley in being a Co-Advisor and proofing my thesis.

Lastly, the author would like to thank Mr. Glenn Harrell. Mr. Harrell provided all machining requirements for the demonstration refrigerator. His attention to detail and sound advice helped to produce quality parts with no wasted man-hours.



## **I. INTRODUCTION**

Thermoacoustics is a relatively new area of heat engine research and promises to be an important field well into the future. In the last ten years many advances have been made in the area of thermoacoustic refrigeration. Generation of cooling power from acoustic power offers an important alternative to the current usage of ozone damaging chlorofluorocarbons (CFC's) within refrigerators of today's technology. In depth research concerning thermoacoustic refrigeration can be found at the Naval Postgraduate School within the Physics Department.

### **A. THERMOACOUSTIC REFRIGERATION**

Typically, a thermoacoustic refrigerator uses an acoustic driver to produce a standing wave in a one quarter wavelength resonant tube. The driver functions like a loudspeaker creating sound from electricity. If a suitable layered stack structure is appropriately placed near the pressure antinode of the standing wave, a transfer of heat will occur between opposite ends of the stack. The stack structure is actually a multilayered (rolled) combination of polyester plastic film and monofilament line used as spacer between layers. See Fig. 1. The layers create channels through which the acoustic wave travels. They are parallel to the wave propagation direction and serve as a conduit for the transfer of heat and acoustic power. Of course, some acoustic power is dissipated in the channels by the heat transport process. A more detailed explanation of a gas parcel model of the heat transfer process can be found in [Ref. 1, 2, 3, 4]. Instead of repeating this physical model again, a brief functional description of the stack in its acoustic environment will be given.

A standing wave exists in the resonant tube containing a stack. The quality factor of the resonance is in the range of 10 to 30. One end of the stack is placed very near a pressure antinode of the standing wave. This distance is typically about  $1/50$  of a wavelength, and the length of the stack is roughly  $1/50$  of a wavelength. The interaction



between the oscillating gas in the channels of the stack, and the stack surface causes heat to be transported from one end of the stack to the other. The direction of the heat transport is towards the nearby pressure antinode.

The size of a single channel cross-section is typically two to four thermal penetration depths,  $\delta_k = \sqrt{2\chi/\omega}$ , where  $\delta_k$  is approximately the distance that heat can diffuse in one acoustic cycle,  $\chi$  is the thermal diffusivity of the gas, and  $\omega$  is the radian frequency. The compression and expansion of the gas in the channel are neither isothermal nor adiabatic. Therefore, temperature oscillations exist and heat also flows (diffuses) transversely between the gas and the adjacent solid surface area. The spacing of a few  $\delta_k$  leads to temperature oscillations in the gas that are not in phase with the acoustic pressure oscillations. This phase shift between pressure and temperature leads to a non-zero time average heat flow along the stack surface.

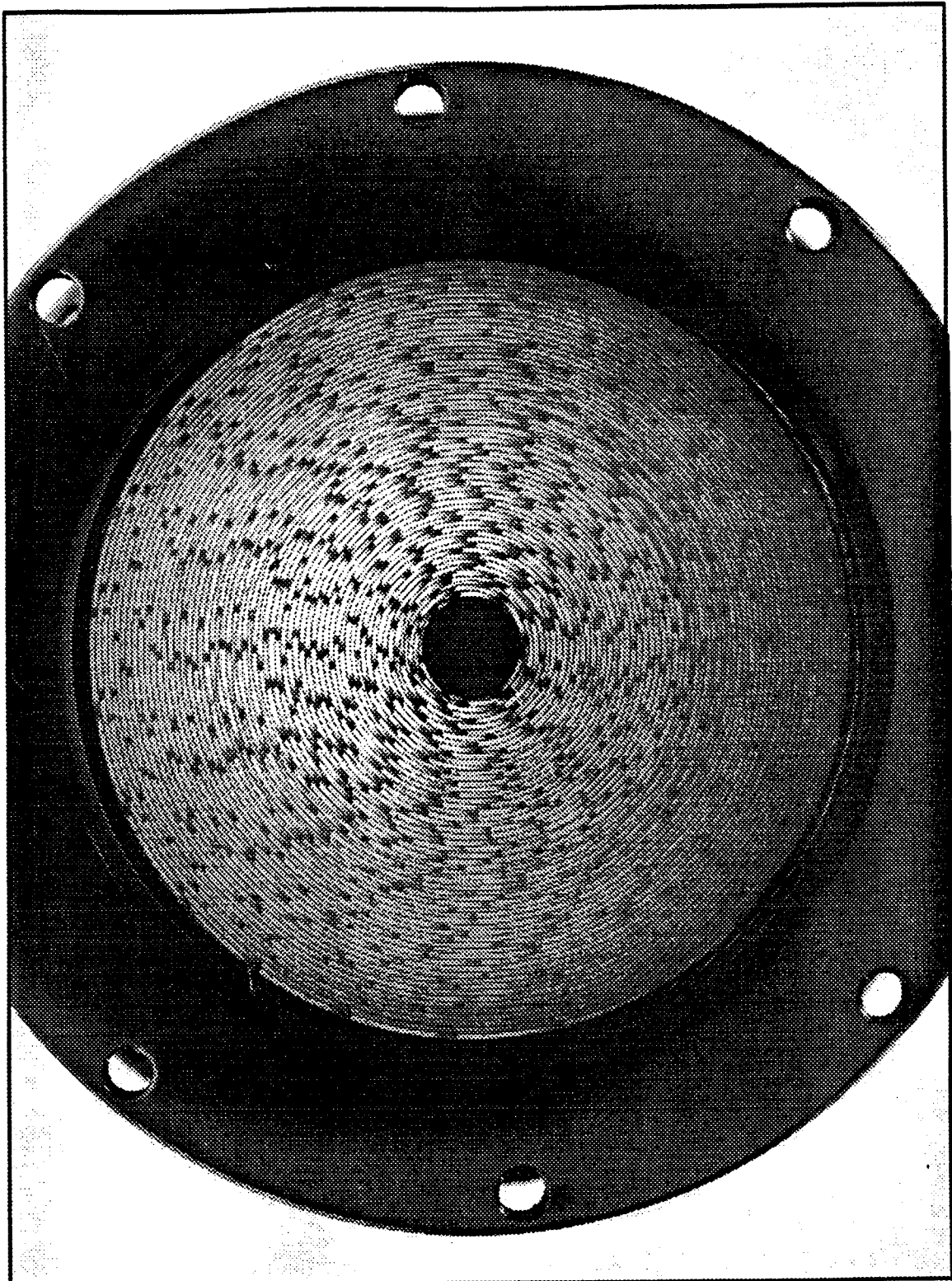


Figure 1. Thermoacoustic Stack

## **B. HISTORY OF THERMOACOUSTIC REFRIGERATORS**

### **1. The Hofler Refrigerator.**

As part of Dr. Hofler's doctorate program, he built an experimental refrigerator at the Los Alamos National Laboratory. The model reached a low temperature of 200° K starting at 300° K [Ref. 3]. Hofler's refrigerator, which will be discussed in more detail later, is the basis for subsequent refrigerators used in follow-on projects including the demonstration refrigerator used in this thesis.

### **2. The Space Thermoacoustic Refrigerator (STAR).**

As part of a research team Dr. Hofler joined forces with Dr. Steve Garrett, Mr. Jay Adeff, and several students to design and build an experimental refrigerator flown on board the space shuttle. The device was appropriately named the Space Thermoacoustic Refrigerator or (STAR). Dr. Garrett was the principle investigator, Dr. Hofler was the chief scientist, and Mr. Adeff was the principle engineer. STAR was tested on the space shuttle flight STS 42. See Fig. 2. [Ref. 5]

### **3. An Early Demonstration Refrigerator.**

A demonstration refrigerator was later built by Hofler and associates for a demonstration at an Acoustical Society of America meeting. The demonstration model produced a cold temperature of 8.9° C [Ref. 6]. The cold end temperature was observed on a thermometer via a thermocouple. This unit was simple and cheap to build, but the cooling effect was weak and could only be detected with a thermometer. See Fig. 3.

### **4. The Brooks Demonstration Refrigerator.**

The early demonstration refrigerator failed to bring about a graphic display of the phenomena. It was decided to build a more impressive demonstration refrigerator and a

new set of objectives was established. These objectives provided the basis for Lt. Brook's thesis [Ref. 7] and this thesis. The objectives were to design, construct and operate a portable thermoacoustic refrigerator capable of producing frost on an exposed and readily visible metal surface for lecture demonstrations.

The majority of parts and components were designed and built by a previous thesis student, Lt. Brent Brooks. The purpose of this thesis was to complete construction of a few components, assemble the unit, and test and measure its characteristics and performance.

Chapter II discusses the basic objectives and the design of the demonstration refrigerator. Topics include design parameters required to optimize its performance, the need for compactness for portability and the need for effective air cooling of the entire unit.

Chapter III contains a discussion of the performance. The initial measurements were done with recirculating water cooling the driver and hot heat exchanger. Subsequent measurements were done with air cooling. Both electrical driver impedance and acoustic impedance measurements were performed as functions of frequency at different cold end temperatures. These measurements were done with an insulated resonator tube and an uninsulated resonator. Temperatures as functions of time were also measured to illustrate the refrigerator's performance, and to determine the efficiency. Lastly, heat loads were introduced with steady state cooling as an alternative method of measuring efficiency.

Chapter IV elaborates on the packaging of the portable refrigerator. Descriptions are given of the portable circuitry to drive the refrigerator, the carrying case, thermocouples, and thermometers for temperature readouts.

Chapter V relates some thoughts and conclusions based on the work accomplished, suggesting areas of improvement.

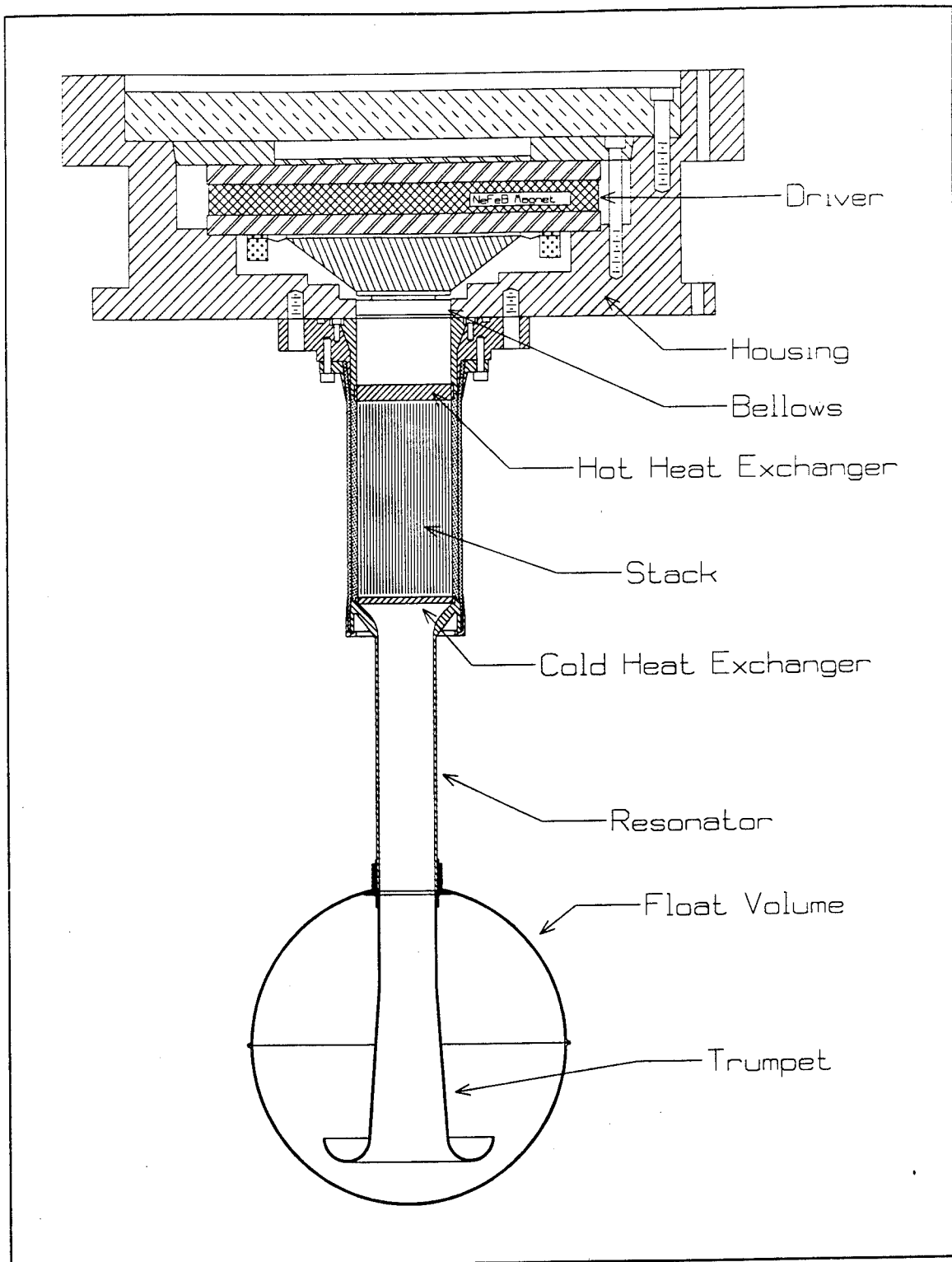


Figure 2. Space Thermoacoustic Refrigerator (S.T.A.R.)

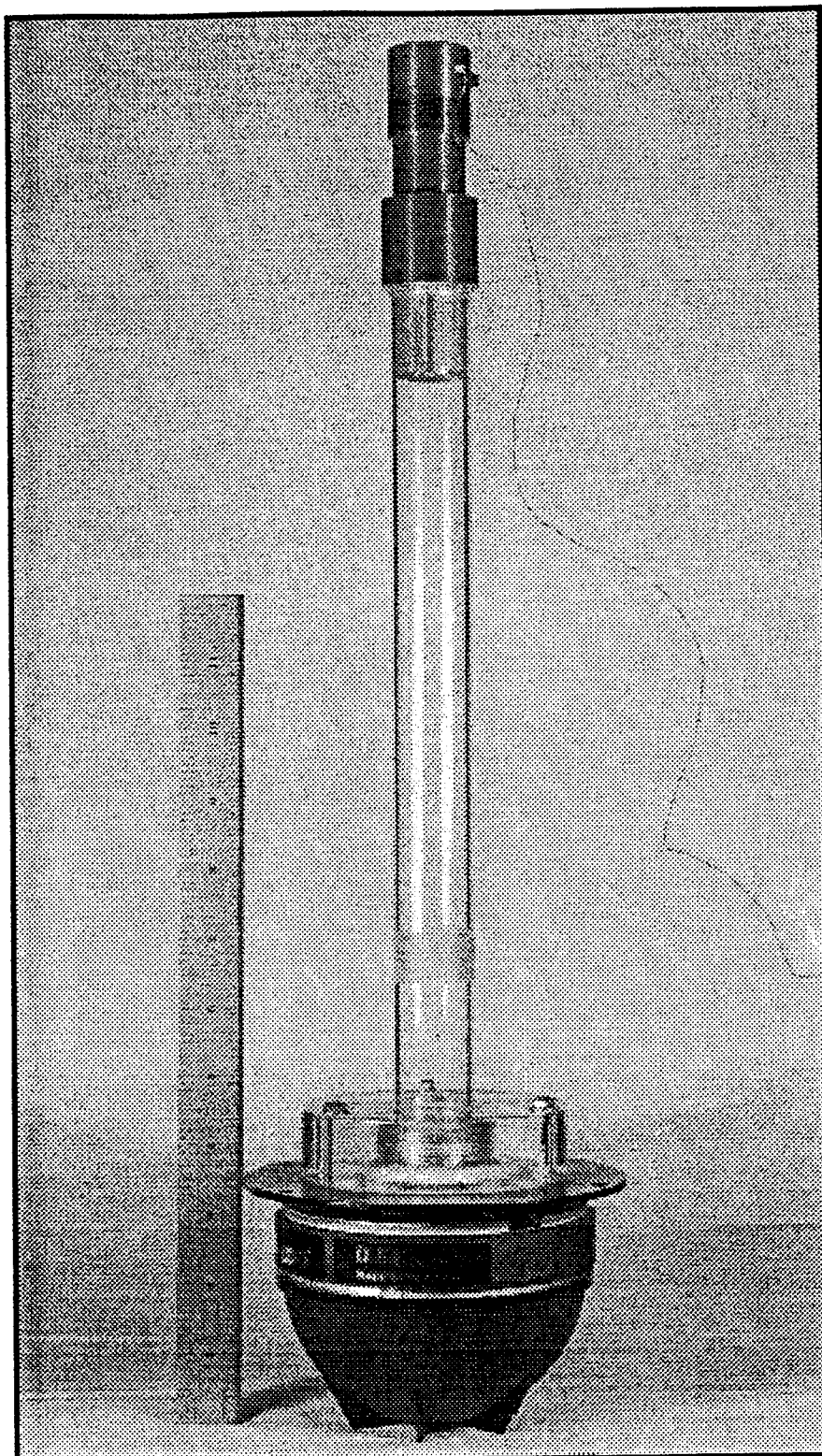


Figure 3. Original Lucite "Demo-Frig"



## **II. DEMONSTRATION REFRIGERATOR**

### **A. OBJECTIVES OF THE NEW REFRIGERATOR**

#### **1. Cold/Frosted Metal Part.**

The demonstration refrigerator must produce an ice build up on a metal surface that can be both seen and touched. In addition, the ice build up must occur in under 15 minutes and in a lecture sized auditorium.

The first and foremost objective was that the apparatus reach a temperature below  $0^{\circ}\text{C}$  in order for frost to develop on the cold end. To achieve this in a room with an ambient temperature of  $25^{\circ}\text{C}$ , the stack needs to produce at least a  $40^{\circ}\text{C}$  temperature span. The need for a  $40^{\circ}\text{C}$  span is to allow for unavoidable temperature differences within the internal heat exchangers and the final heat exchange to the room air.

A second criteria, which is critically tied to the first, is that sufficient cooling power must be available for the refrigerator to produce a frosted surface. Previous calculations indicate that ten watts should be sufficient for rapid cool down and for removing any heat entering into the system from the environment. [Ref. 7]

#### **2. Compact/Portable Demonstration Model.**

A major criteria for this refrigerator was the portability and compactness of the entire unit, which required keeping the weight and overall size to a minimum. The ancillary support equipment to operate the demonstration unit outside of the laboratory environment are all integral parts of the device and must be small enough to fit in a hard shelled suitcase.

#### **3. Air Cooled Operation.**

As part of the portability requirement, as well as for simplicity, the unit was also designed to be air-cooled and not water cooled, which is the typical means used in a



laboratory environment. The water cooled method utilizes copper tubing wrapped around the circumference of the driver. Water is pumped through the tubing, and heat is transferred via conduction to the copper tubing and ultimately the water. This method does not allow the refrigerator to be mobile. With air cooling the demonstration refrigerator can be moved and operated in virtually any location. The specifics of the design are covered in the following design section.

## **B. BASIC DESIGN**

### **1. Mode/Adeff Acoustic Driver.**

The Mode/Adeff acoustic driver is used in the operation of the demonstration refrigerator. The Mode/Adeff acoustic driver borrows features from the original Hofler and STAR drivers. These two drivers provided an excellent starting point for making a robust demonstration refrigerator driver. The Hofler thesis and STAR driver performances were well characterized. Lastly, the Mode/Adeff acoustic driver met the needs for a more compact, lighter and easier-to-service portable unit, which was desirable from a packaging perspective. See Fig. 4. [Ref. 8]

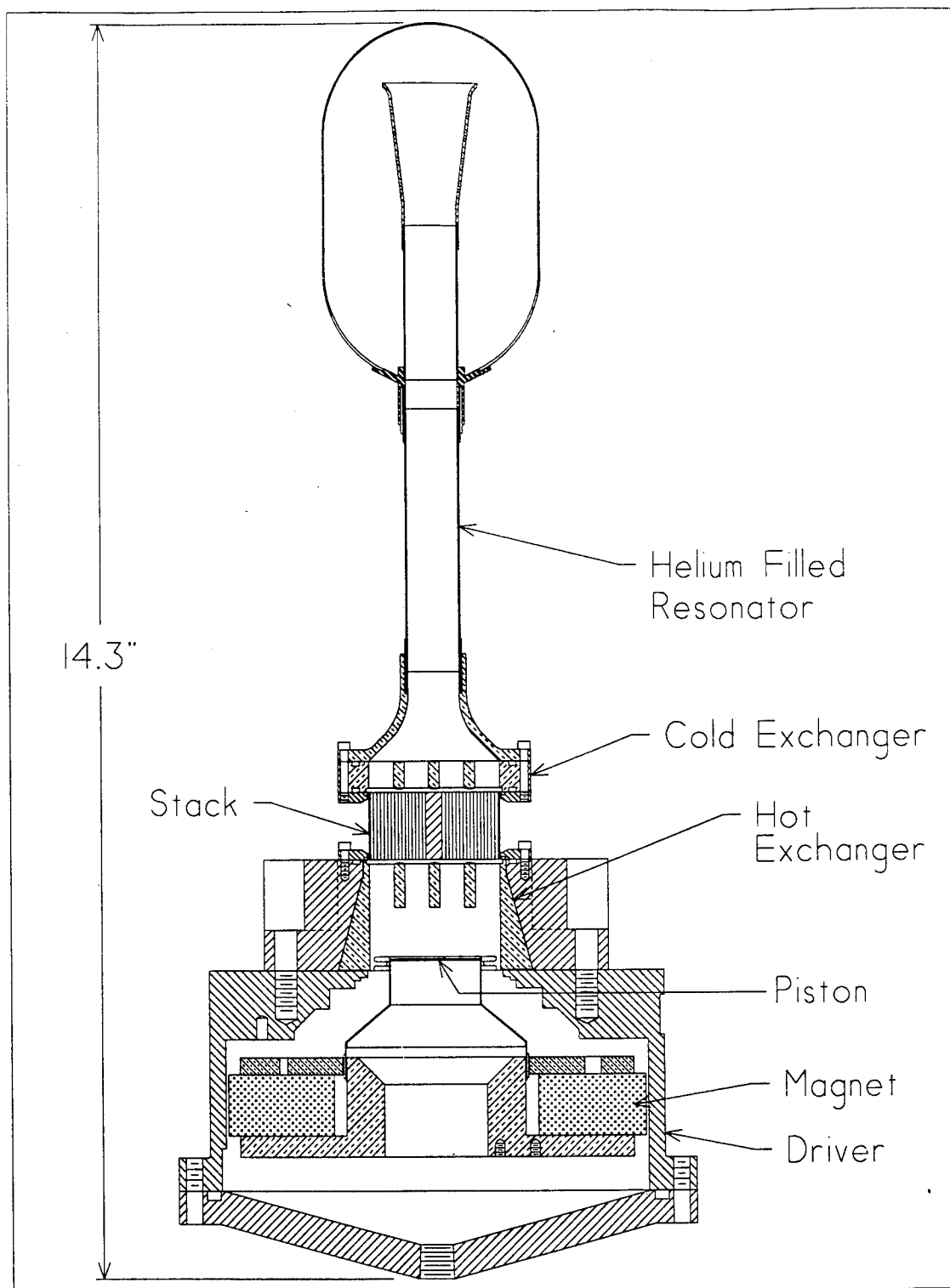


Figure 4. Demonstration Refrigerator Section

## **2. Brooks Resonator.**

The next sub-system of the demonstration refrigerator was the design of the resonator. The resonator was designed, parameterized, and built by Lt. Brent Brooks, Dr. Tom Hofler, and Mr. Jay Adeff. A brief explanation of the key individual components will provide an understanding of the overall operation of the refrigerator. See Fig. 4.

### ***a. Resonator Parameters.***

The resonator was specifically designed with a higher frequency range than previous designs. More precisely, a nominal range of 650 Hz was targeted, which is the upper practical limit for the driver. Helium was chosen as the working medium, with a mean pressure of 90 psia. The temperature span was targeted at 40° C to achieve a cold temperature of at least a -5° C to ensure frost buildup at the cold end. Forty degree Celsius was chosen assuming a total 10° C temperature defect for all heat exchange and an ambient temperature of 25° C. In addition, by computer model, the small resonator tube outer diameter (o.d.) of 3/4 in. was found to be optimal for minimizing acoustic losses. A diameter of 5/8 in., however, was actually used because it decreased the overall length of the resonator by 2.7 inches while only slightly increasing acoustic losses. Lt. Brooks concluded that the small reduction in the resonator tube diameter would decrease the overall efficiency only slightly as a result of the higher acoustic velocities and the higher viscous losses. Since the resonator would be exposed to a room environment instead of a vacuum chamber, a thin walled stainless steel tube (wall thickness 0.016 in.) was chosen to minimize the heat load on the cold heat exchanger. The use of thin walled stainless steel will also minimize heat transfer in case the tube itself warmed up due to viscous losses in the gas. This is explained by Adeff and Brooks. [Ref. 5, 7]

### *b. Optimized Parameters.*

Three critical parameters concerning the stack were optimized by Lt. Brooks: stack position, stack length, and stack layer spacing. A thermoacoustic refrigerator design requires the stack be placed somewhere near a pressure antinode of the standing wave. This minimizes viscous dissipation in the stack, because the acoustic velocities are small near a pressure antinode. A wave number,  $k_x$ , is defined as  $k_x = 2\pi/\lambda$ . Here  $\lambda$  is the wavelength of the standing wave. For helium at about 650 Hz,  $k_x = 0.04 \text{ cm}^{-1}$ . The wave number  $k_x$  is then multiplied times  $x_{\text{hot}}$ .  $x_{\text{hot}}$  represents the distance from the driver piston surface to the hot heat exchanger. A computer model developed by Dr. Hofler utilizes these dimensionless parameters and calculates the optimal position of the stack. The computer model produced a value  $k_x x_{\text{hot}} = 0.052$  or  $x_{\text{hot}} = 1.3 \text{ cm}$ .

Since the hot heat exchanger includes a substantial length of copper cross bars and copper fins, the actual distance between the driver piston and the hot end of the stack is  $k_x \Delta x = 0.108$  or  $\Delta x = 2.7 \text{ cm}$ . Some of the gas volume in the heat exchanger is occluded with copper, so the effective distance between the driver piston and the hot end of the stack is roughly  $k_x \Delta x = 0.093$  or  $\Delta x = 2.3 \text{ cm}$ .

The next parameter optimized was the stack length. It is the distance between the cold and hot heat exchanger surfaces. It is characterized by wave number  $k_x$  times the stack length,  $x_{\text{stack}}$ . The parameter was found to be  $k_x x_{\text{stack}} = 0.0879$  or  $x_{\text{stack}} = 2.2 \text{ cm}$ .

The last parameter looked at was the stack spacing. Lt. Brooks characterizes this by the ratio  $y_o/\delta_k$ , where  $y_o$  is the half-plate separation and  $\delta_k = 0.0121 \text{ cm}$  is the thermal penetration depth of the gas. The thermal penetration depth is approximately the distance over which heat diffuses in one acoustic cycle. The value  $y_o/\delta_k = 1.050$  was found, so the plate separation is  $2y_o = 0.025 \text{ cm}$ . This parameter was used to get the thickness of the fishing line used to separate each layer of the stack. [Ref. 7]

### *c. Performance Predicted by Optimization.*

The outcome of the computer model, based on iterative runs, was that the optimal stack position was  $x_{\text{hot}} = 1.3$  cm, with a stack length of  $x_{\text{stack}} = 2.2$  cm and a stack spacing of  $2y_o = 0.025$  cm. Because of a drafting error, the actual stack length built was  $x_{\text{stack}} = 2.0$  cm. The coefficient of performance (COP) and coefficient of performance relative to Carnot (COPR) were predicted to be 1.28 and 20.8%, respectively, with an internal temperature span of 40° C. [Ref. 7]

### *d. Finned Heat Exchangers with Crossbars.*

For proper operation, heat must be transferred between the stack and the cold/hot heat exchangers. As mentioned previously, within the stack, heat moves parallel to the axis of the stack/resonator. Within the finned copper heat exchangers, however, heat is transferred at 90° to the axis of the stack/resonator. In other words, heat flows along the fins of the heat exchanger elements. See Fig. 5 & 6.

Since the change in temperature of the copper is a function of distance traveled through the copper fins, the prime objective is to minimize the distance. Within the Brook's resonator this was accomplished by adding copper bus bars directly to the fins of the heat exchanger, which decreased the distance traveled by a factor of four. This distance decrease caused a factor of sixteen reduction in the temperature defect profile. A comparison calculation by Lt. Brooks for heat exchangers with and without bus bars illustrates the significant difference. The total temperature defect was found to be about 5.0° C. Total defect is defined to be the sum of the individual calculated temperature defects for the fins and bus bars for both hot and cold heat exchangers. The calculated 5.0° C loss within the heat exchangers was considered acceptable. [Ref. 7]

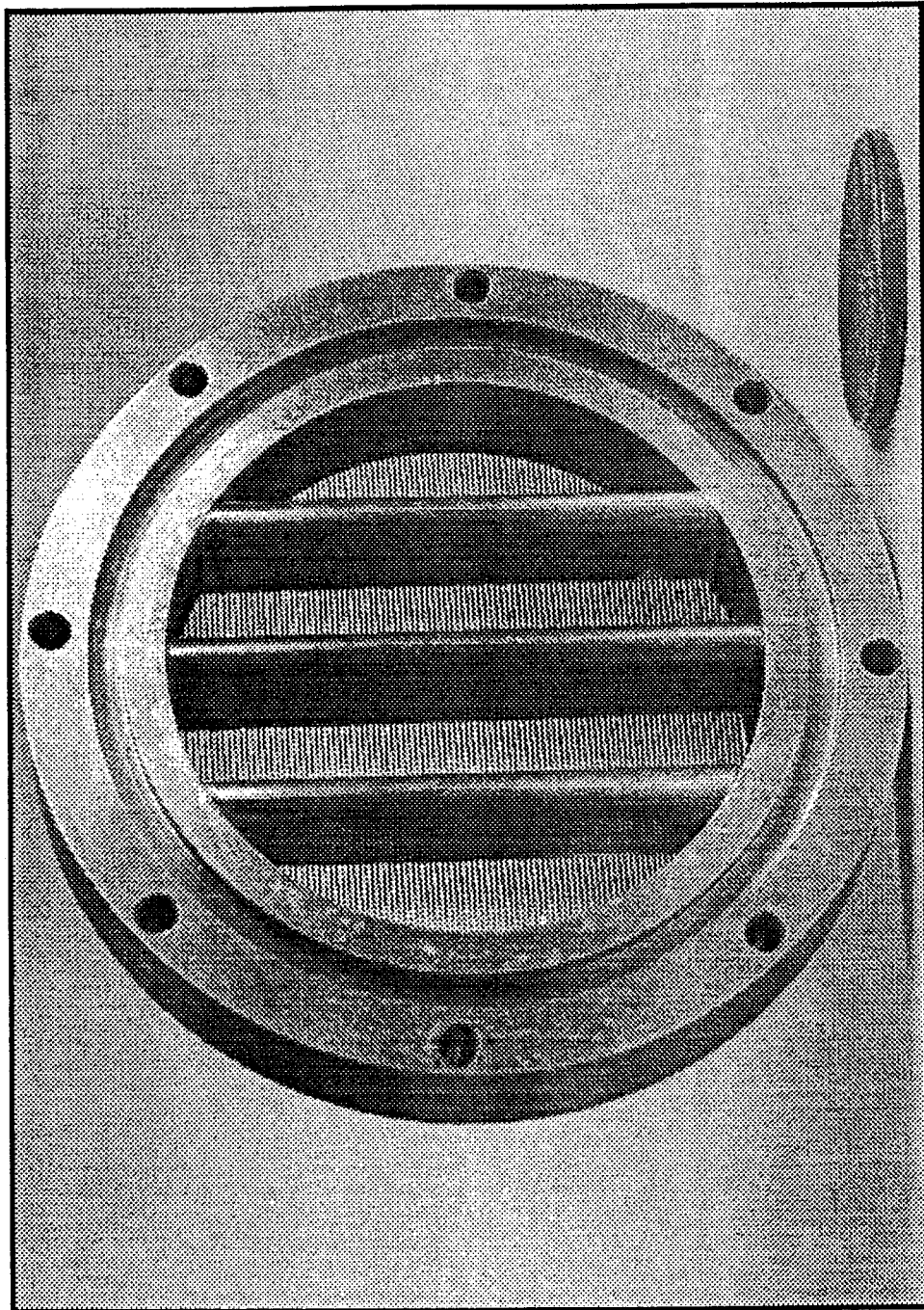


Figure 5. Cold Heat Exchanger

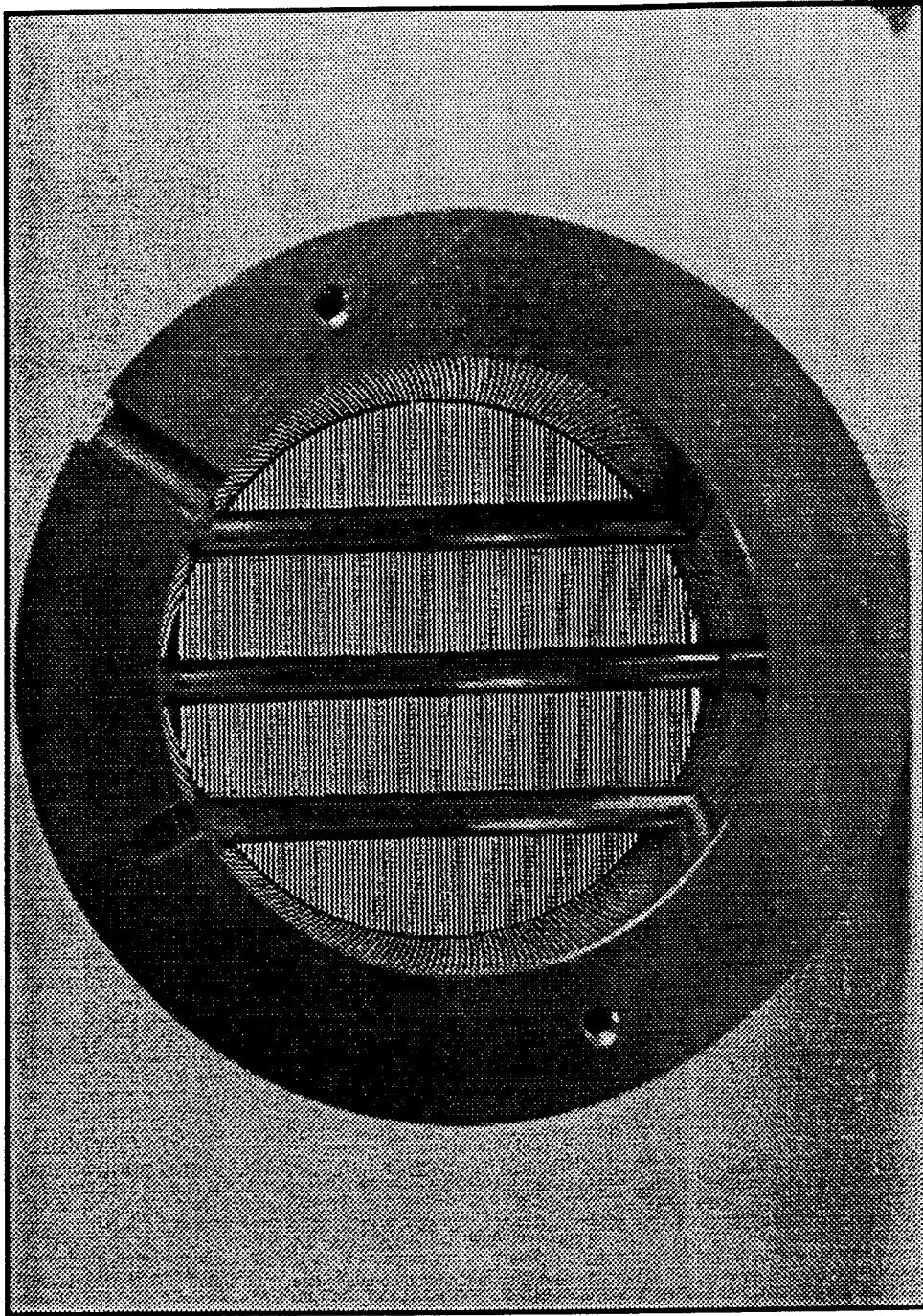


Figure 6. Hot Heat Exchanger

### 3 . Air Duct and Fan.

As mentioned previously, the air cooling of the refrigerator was one of the last remaining obstacles for a portable thermoacoustic demonstration refrigerator. A shroud or cowling was required for proper air cooling with a fan. This shroud would serve as a conduit through which air is drawn from the top, through the aluminum heat sink fins of the hot heat exchanger flange, past the driver housing, and exhausted out the bottom of the shroud. The airflow is provided by a small muffin-type fan located at the bottom of the shroud. The shroud added little to the size and it also allowed portability with the fan accomplishing all cooling requirements. See Fig. 7.

A pressure drop between the air inlet and air outlet was calculated. The following assumptions were used for calculation purposes:

- 1) Circular gap was approximated by two parallel planes.
- 2) Minimum gap size between shroud and acoustic driver was set at 1/4 in.
- 3) Steady state airflow.
- 4) Incompressible gas to simplify calculations.

Using a Navier-Stokes formula taken from a textbook for flow between two parallel planes [Ref. 9], we find:

$$\bar{v} = \frac{h^2}{12\eta} \frac{dP}{dX} \quad 1)$$

Parameters are defined as follows:  $h$  is the gap between acoustic driver flange and shroud, set at 0.25 in.,  $\eta$  is the dynamic viscosity,  $dP/dX$  is the differential pressure per unit change in distance and  $\bar{v}$  is the mean velocity.

$$\dot{V} = ch\bar{v} \quad 2)$$

Here the parameters are defined as follows:  $\dot{V}$  is the volumetric flow rate (chosen to be 35 cfm),  $c$  is the circumference of the driver. Substituting Eq. 2 into Eq. 1 and solving for differential pressure per unit change in distance yields Eq. 3:



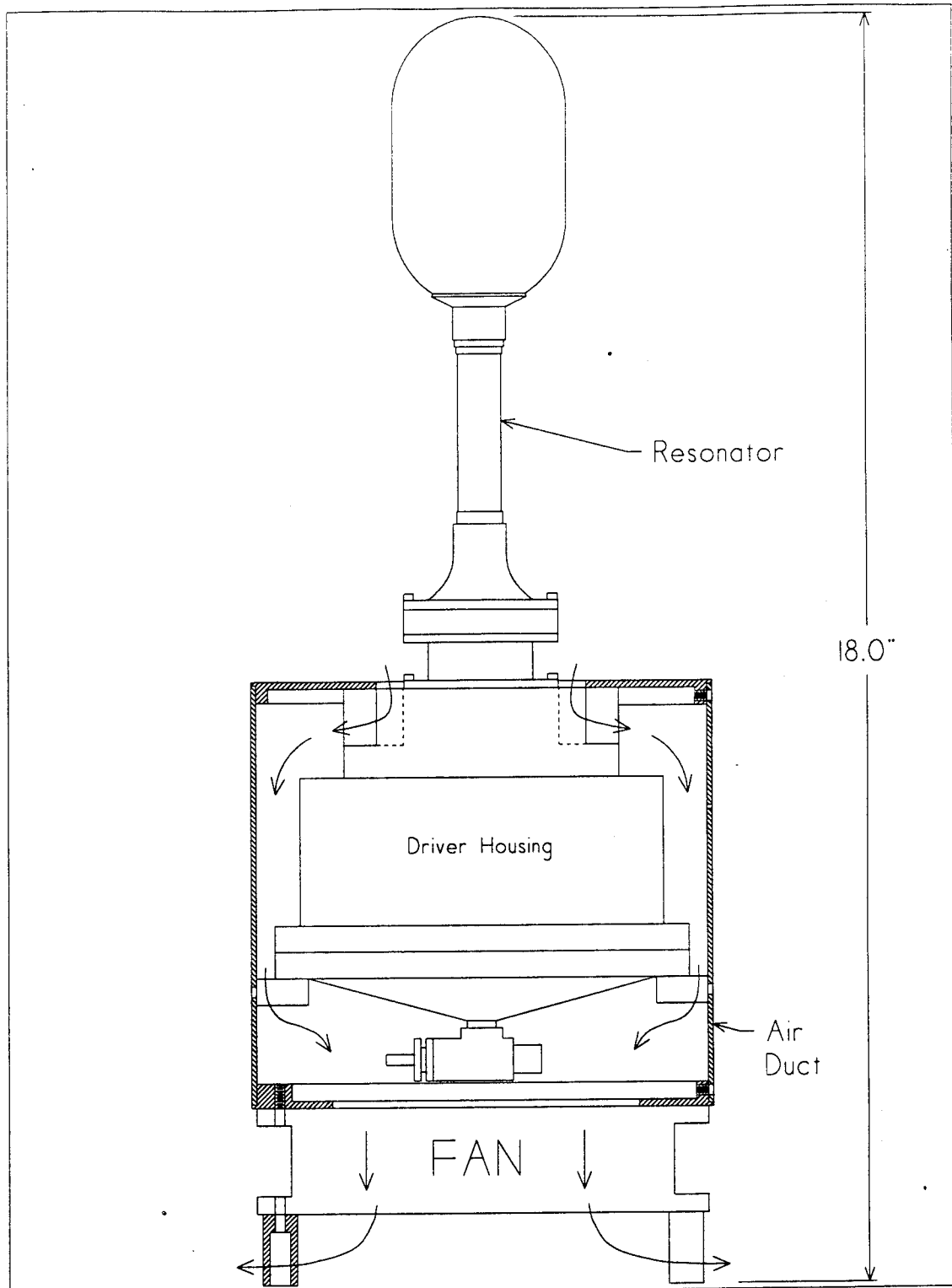


Figure 7. Schematic Airflow for Shroud

$$\frac{dP}{dX} = \frac{12\dot{V}\eta}{ch^3} = \frac{12 \left[ 16500 \frac{cm^3}{sec} \right] \left[ 1.8 \times 10^{-4} \frac{g}{cm-sec} \right]}{(49.87 cm)(0.635 cm)^3} \quad 3)$$

$$\frac{dP}{dX} = 2.79 \frac{dynes}{cm^3} = 27.9 \frac{Pa}{m},$$

Using the previous result and multiplying by the length  $\Delta x$ , a  $\Delta P$  can be found as in Eq. 4:

$$\Delta P \cong \frac{dP}{dX} \Delta x, \Delta x = 1.9 cm \quad 4)$$

$$\Delta P \cong 2.79 \frac{dynes}{cm^3} 1.9 cm = 5.2 \frac{dynes}{cm^2} = 0.52 Pa$$

According to manufacturer's data [Ref. 10], if  $\Delta P$  is below 0.05 in. of water then the fan flow rate is close to its maximum value. A pressure of 0.05 in. of water is about 12 Pa, which is much greater than 0.52 Pa. Based on this fact, the flow impedance of the shroud was sufficiently low. Actual fans purchased were capable of producing 34 cfm (slow fan) and 105 cfm (fast fan). Experimental test runs conducted with these two different speed fans will be elaborated on in the following chapter. Additional computer aided design drawings (CADD) of the individual shroud components are located in the appendix.



### III. MEASUREMENTS

Prior to operational testing, the demonstration refrigerator was tested for gas leaks. Ideally, the leakage should be zero; however, because helium can diffuse through materials used in the electrical feedthroughs and rubber O-ring seals, a small leakage rate of helium does occur. The leakage is small and does not prevent the operation of the refrigerator.

#### A. FIRST REFRIGERATION TESTS

The short term goal of these initial tests is to see if frost could be produced on the outside of the cold heat exchanger and copper reducer. First the unit was purged with helium and pressurized to 76.5 psig. The purging consists of slowly cycling the pressure from 0 psig to roughly 100 psig and back again, several times. Because the hardware for air cooling the apparatus was not ready, a recirculating water chiller was used to remove the heat being rejected by the refrigerator as well as the electrical heating in the driver. The recirculating water flowed through coils of copper tubing wound around the driver housing and the hot heat exchanger flange of the acoustic resonator. The apparatus was connected to instrumentation that provides electrical power to the driver and enables measurement of acoustic impedance inside the resonator at high acoustic amplitudes, while refrigeration is occurring.

Transducers are mounted in the driver for the measurement of acoustic impedance [Ref. 8]. These consist of a dynamic pressure transducer ported to the resonator volume at a location adjacent to the driver piston and a sub-miniature accelerometer attached to the piston. With appropriate calibrations [Ref. 11], the acoustic pressure and volume velocity delivered by the piston to the load impedance represented by the resonator can be accurately measured over the limited frequency range of interest (250 to 750 Hz). Note the relative phase between acoustic pressure and volume velocity is calibrated and can be measured accurately. These types of acoustic measurements are used in some of the following tests.

With the system pressurized and at room temperature, the resonant frequency was determined to be about 640 Hz. The resonant frequency is typically defined to be that frequency which makes the acoustic pressure and volume velocity in phase at the driver piston [Ref. 12]. This is equivalent to placing the pressure antinode of the standing wave at the position of the driving piston. After determining the resonant frequency, the current to the driver was increased to about 2 A rms. The peak acoustic pressure amplitude achieved was 5% of the mean internal pressure. Within less than 20 minutes frost was observed on the uninsulated copper reducer. The outcome of the initial test was a success and the primary goal had been achieved. We were relatively certain that it would work with air cooling as well. See Fig. 8.

On the initial test run one notable observation was made. Typically, the resonant operating frequency is tracked with a phase-locked-loop circuit that precisely maintains zero acoustic phase at the driver piston. In previous large temperature span (100° C) refrigerators the frequency change during cool-down was as much as 20%. In this initial test, as the cold heat exchanger and copper reducer parts cooled down in temperature, there was very little change in resonant frequency. The total frequency variation was less than one percent.

The amount of frequency change with respect to temperature was much smaller than we anticipated, even when the reduced temperature span of this refrigerator is taken into account. The reason for this is because the cold temperatures of the resonator are limited to the region near the cold heat exchanger. The density of the high acoustic velocity gas is the primary factor in determining the change in the resonant frequency, and the high acoustic velocities are primarily in the small diameter tube of the resonator. Except for a small portion at the copper reducer (which is directly above the cold heat exchanger), most of this small diameter stainless steel tube is closer to room temperature than it is to the cold temperature. In previous designs all of the small diameter tube is cold. This feature was intentionally designed into this refrigerator so that the heat leak



Figure 8. Frosted Cold Heat Exchanger

from the room to the cold heat exchanger would not be too large. Apparently it also results in a minimal frequency shift with respect to the cold temperature.

## **B. ELECTRICAL IMPEDANCE MEASUREMENTS**

### **1. Uninsulated Resonator at Different Temperatures.**

Starting with the resonant frequency of 640 Hz just described, additional testing was conducted to find the best operating frequency. Low amplitude frequency sweeps were conducted with an impedance analyzer<sup>(2)</sup> connected to the electrical terminals of the driver. The frequency intervals were set at 2 Hz steps. Two sweeps were conducted on the uninsulated resonator. The first was performed with the cold heat exchanger at the coldest operating temperature and the second was performed with all of the resonator at room temperature. These measurements are plotted in Fig. 9 & 10 respectively. The magnitude of the two impedance peaks is in the range of 8.5 to 9.5 ohms. This information is valuable in determining the requirements for the portable power amplifier. The frequency of the electrical impedance peak is at about 665 Hz in both of the these plots. This also indicates that the electric to acoustic efficiency of the driver will be maximum at about 665 Hz.

The reason for the correspondence between the frequency of maximum electrical impedance and the frequency of maximum driver efficiency, and for its higher value than the previous resonant frequency of 640 Hz, is somewhat involved. Prior to this thesis, direct measurements of electric to acoustic efficiencies for this driver were performed with a test resonator [Ref. 13]. These measurements showed the connection between electrical impedance and driver efficiency. It is beyond the scope of this thesis to reproduce these measurements, and we will only provide a few arguments as justification.

The driver has a natural mechanical resonance in the range of 250 Hz. If we ignore the acoustic load impedance of the resonator, then at a frequency in the range of 650 Hz, the reactance of the moving piston mass dominates the reactance of the driver's

suspension stiffness. Much of the electromagnetic force of the driver is thus wasted accelerating piston mass. If we now consider the effect of the acoustic impedance of the resonator, then at a frequency of exactly 640 Hz, the situation is not changed much, because the resonator provides a purely resistive load. It has a simple damping effect. However, at a slightly higher frequency of 665 Hz, the resonator impedance has a substantial stiffness reactance that can cancel the mass reactance of the driver. In other words, the resonance of the resonator by itself is at 640 Hz, but the resonance of the combined driver/resonator system is at 665 Hz. Driving at this latter frequency, nearly all of the electromagnetic force of the driver is delivered to the acoustic load of the resonator.

When driving at this combined system resonance, the most piston motion is produced with least amount of force. The force is proportional to electrical current. High piston velocities also mean that the electrical coil has a high velocity in the field of the magnet. This produces a "back electromotive force" or an extra voltage. Thus a high voltage and low current occurs at the combined system resonance resulting in a high electrical impedance.



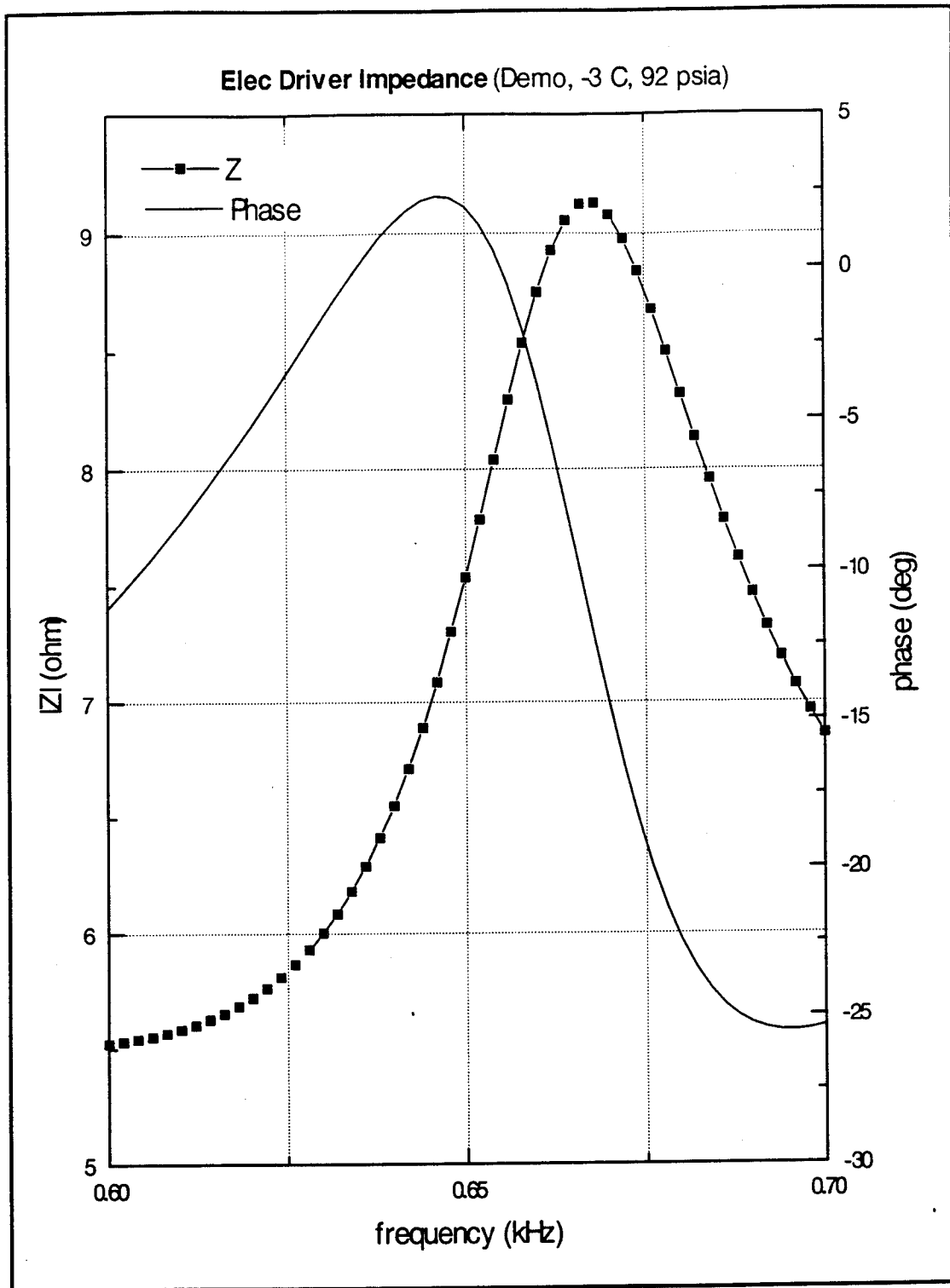


Figure 9. Electric Driver Impedance at Cold Operating Temp., Uninsulated

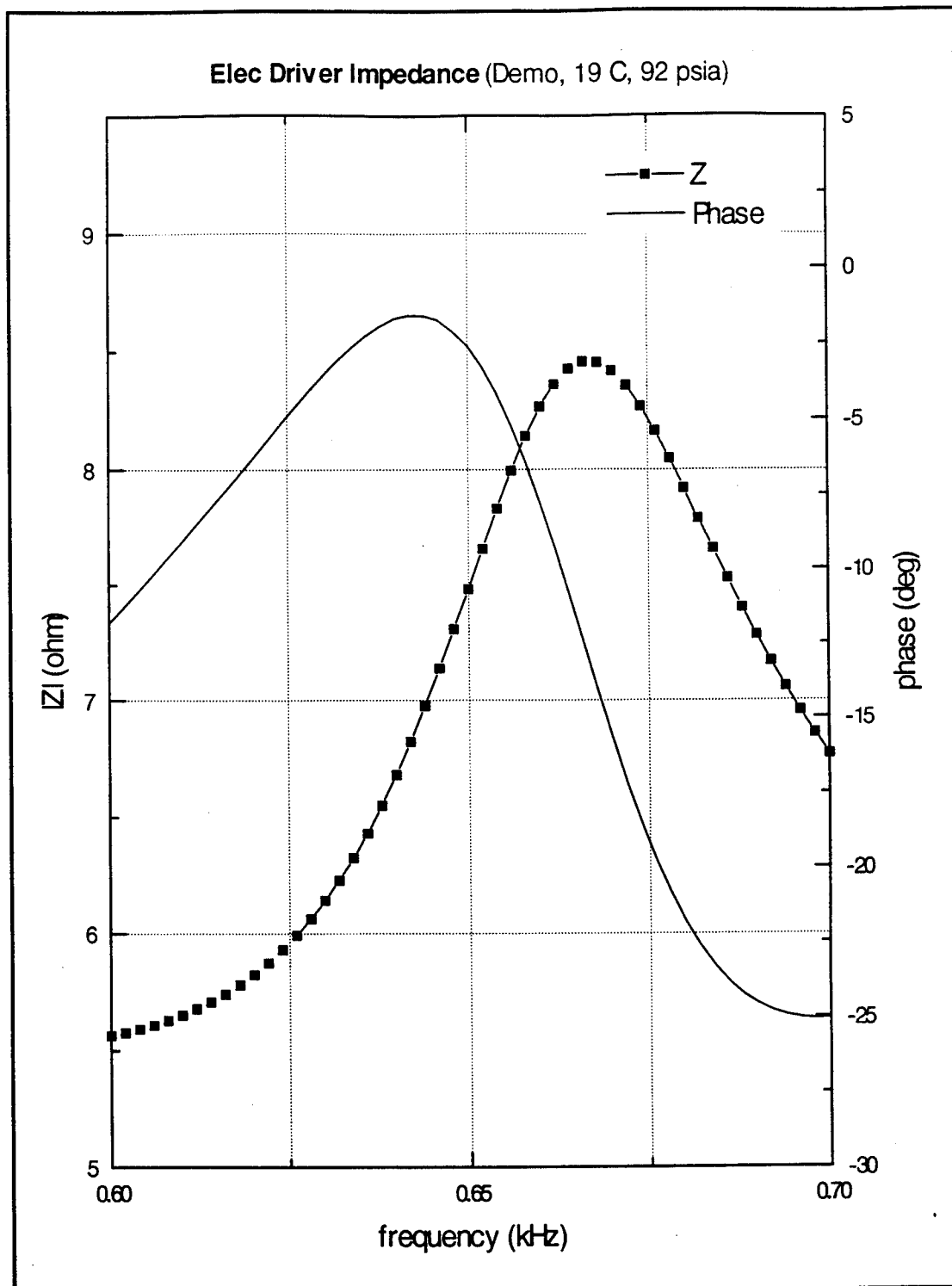


Figure 10. Electric Impedance at Warm Operating Temp., Uninsulated

## **2. Insulated Resonator at Different Temperatures.**

Although the demonstration refrigerator was intended to run without any thermal insulation, we decided to wrap a small amount of insulation on the resonator because we were having difficulty obtaining good quality thermal data. These problems and the insulation is described in more detail below in section C.

Because of the insulation, the temperature distribution along the resonator is altered. In general, the temperatures along the small diameter tube and the float volume become colder because of the reduced heat leak. The colder temperatures may cause shifts in the resonant frequencies, which required the above measurements to be repeated.

The change in resonant frequency associated with the acoustic impedance of the insulated resonator was measured as a function of cold temperature. This data is shown in Fig. 11. These measurements were conducted during full amplitude operation of the refrigerator and are based on maintaining zero phase between dynamic pressure and velocity at the driver piston. The resonant frequency of the insulated resonator does shift slightly with cold temperature and is in the range of 632 Hz to 638 Hz.

Frequency sweeps of the electrical impedance of the driver were also performed again for the insulated resonator both in the cold and warm states. These are shown in Figs. 12 and 13. Notice that the peak-center frequencies for this system resonance are slightly lower than in the uninsulated version and shifts slightly with cold temperature. The peak frequencies are 660 Hz in the warm state and 655 Hz in the cold state.

That the peak frequencies shift more with temperature with the insulated resonator is to be expected since more of the small diameter resonator tube becomes cold and also because the cold temperatures are colder ( $-11^{\circ}\text{C}$  versus  $-3^{\circ}\text{C}$ ). Note also that the 660 Hz peak frequency in the warm state is slightly lower than the 665 Hz peak frequency measured for the uninsulated in the warm state. This small frequency shift was unexpected and unexplained until all of the measurements for this thesis had been completed. The reason behind it is mentioned in the conclusions chapter.

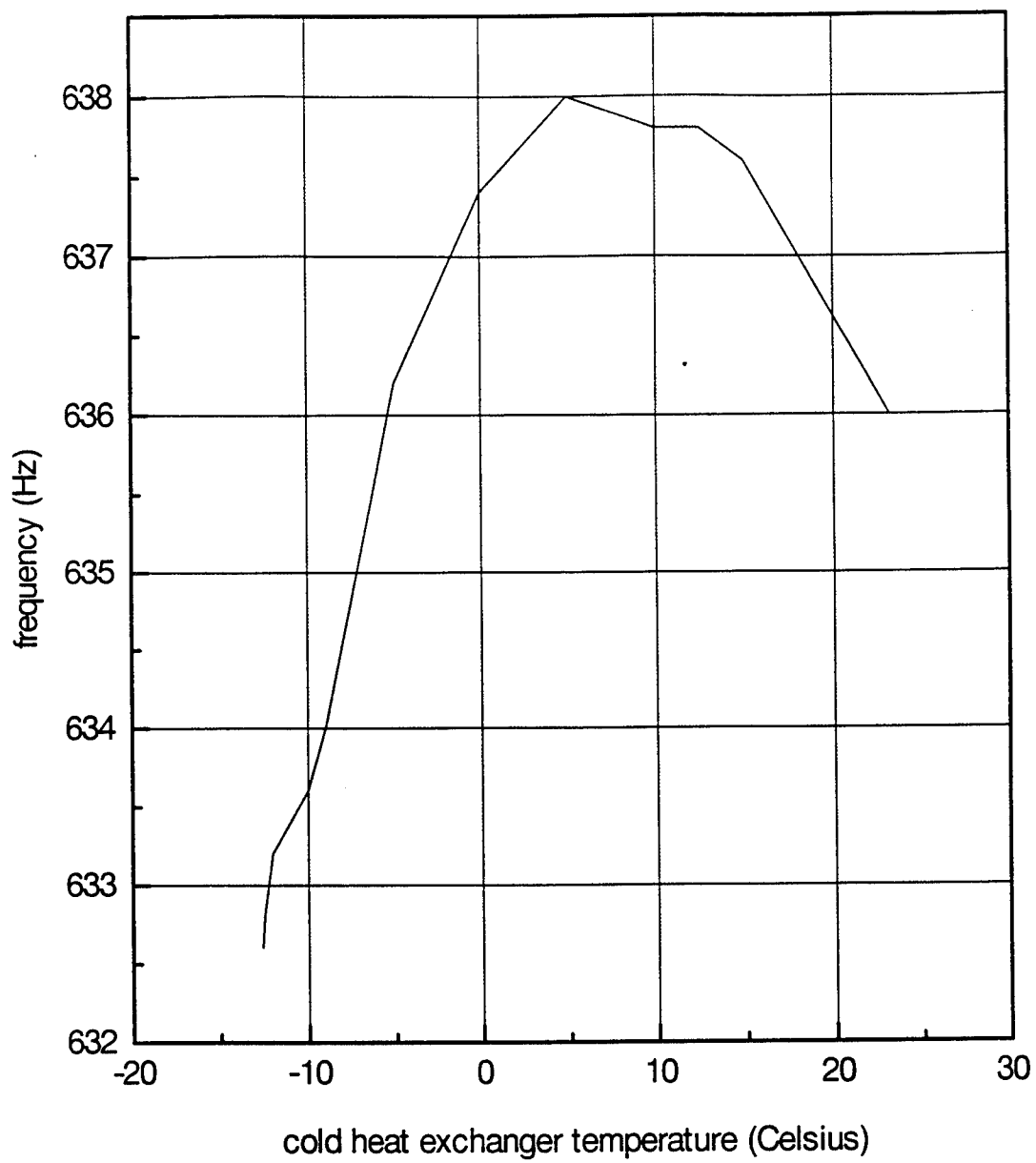


Figure 11. Acoustic Resonant Frequency versus Temperature. The mean pressure was 90 psia and phase between dynamic pressure and acceleration was -90 degrees.

Elec Driver Impedance (Demo, -11 C, 90 psia, 8/8/94)

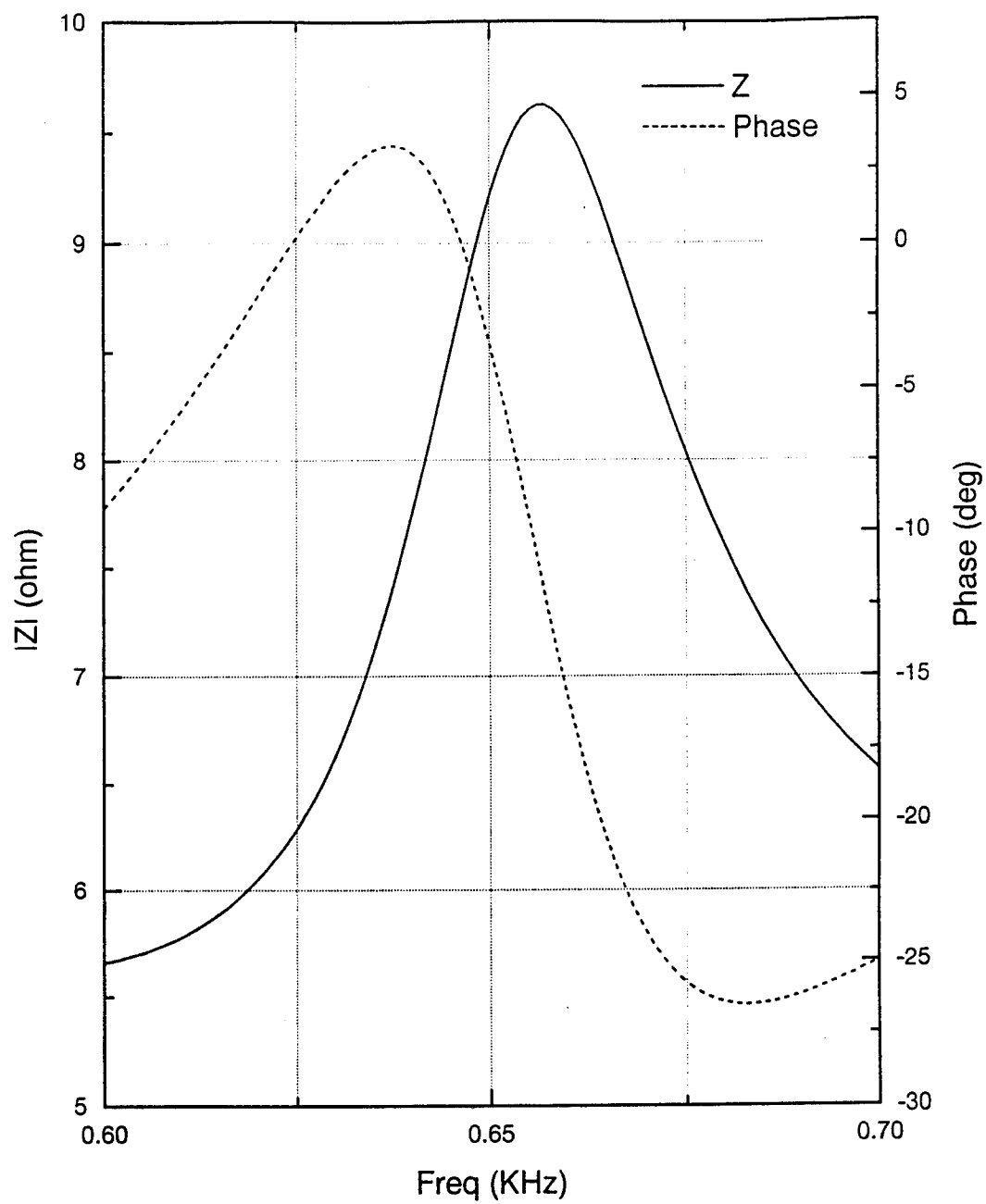


Figure 12. Electric Impedance at Cold Operating Temp., Insulated

Elec Driver Impedance (Demo, 22.6 C, 90 psia 8/8/94)

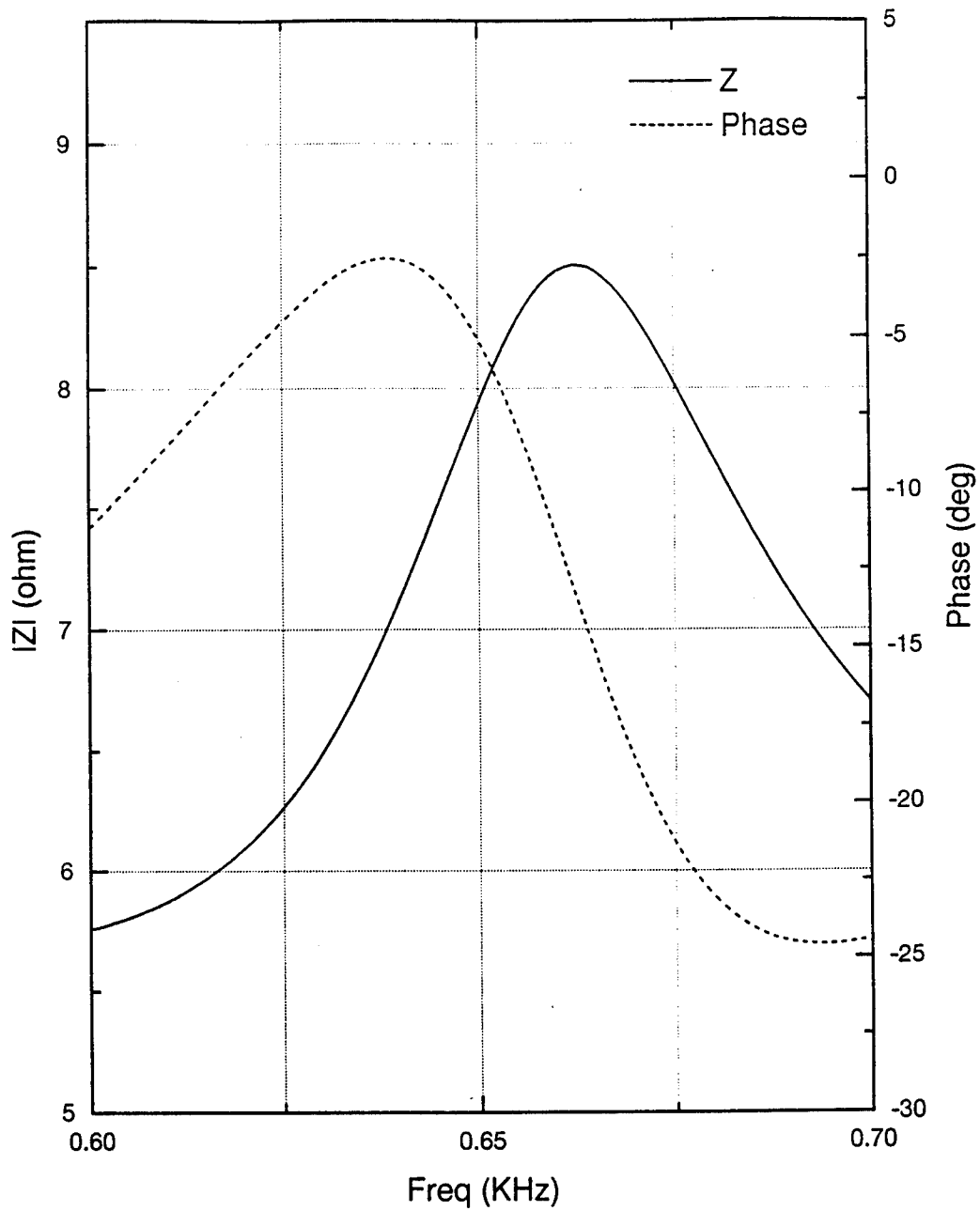


Figure 13. Electric Impedance at Warm Operating Temp., Insulated

## C. TEMPERATURE AS A FUNCTION OF TIME

### 1. Measurement Conditions.

The first measurements of refrigeration performance were simple temperature measurements as a function of time under constant drive conditions. Typically, the driver was run at a constant frequency and at a constant current level for each data run.

The experimental setup utilized a multimeter<sup>(3)</sup> for drive current measurement, a function generator<sup>(4)</sup> and power amplifier,<sup>(1)</sup> and a scanning thermocouple thermometer.<sup>(5)</sup> Temperature data was acquired from the scanning thermometer with a computer. The frequency was set at 665 Hz for an uninsulated resonator and 655 Hz for the insulated version. The driver current was approximately 1.85 A rms. The demonstration refrigerator was allowed to cool down from room temperature for approximately 25 to 30 minutes. This ensured that the cold temperature had achieved a relatively stable value at the coldest level. At this point, the power amplifier was turned off and the unit would be allowed to warm up over the next 35 to 45 minutes, until the cold temperatures were nearly back at room temperature again. During this entire time temperature data was being recorded at fixed time intervals. The temperatures recorded were taken from six thermocouples. The thermocouples were placed at the following locations (See Fig. 4 for clarification).

- 1) Acoustic driver top (located just inside shroud below Aluminum flange).
- 2) Aluminum fin heat exchanger (located on fin of exchanger).
- 3) Cold heat exchanger (located on side of heat exchanger).
- 4) Float fitting (located on fitting that couples the float to the small tube of resonator).
- 5) Top of resonator (located on top of float).
- 6) Room temperature reference.

## 2. Uninsulated and Insulated Resonator Measurements.

An early time dependent temperature measurement with the uninsulated refrigerator is shown in Fig. 14. For this experiment, air cooling of the refrigerator was used. One initial problem was that the air flowing towards the intake of the aluminum finned heat sink also impinges on the cold heat exchanger parts, adding a large heat load. In order to prevent this, an air deflector plate was installed just below the cold heat exchanger. This prevents direct airflow across the cold heat exchanger. For the initial tests the deflector was a piece of cardboard.

The temperature of the cold heat exchanger is the lowest plotted curve in Fig. 14. An important feature of this curve is a small spike from about  $-3^{\circ}\text{C}$  to  $0^{\circ}\text{C}$  on the cool-down portion, and a smaller kink in the warm-up portion of this curve at  $0^{\circ}\text{C}$ . These two features represent the refrigerator making ice from air condensation and the melting of this ice, respectively. It is interesting to note that the water condensation apparently "super-cools" to  $-3^{\circ}\text{C}$  for eight or nine minutes before freezing. The melting kink occurs exactly at  $0^{\circ}\text{C}$ , confirming that the thermometry is accurate. We wanted to fit this temperature data to an exponential function (for reasons discussed in the next section), but these freezing/melting features prevented accurate curve fitting. We decided to apply some thermal insulation to the resonator and attempt to block the air moisture from the cold part in order to improve the quality of the data.

First the cold heat exchanger was surrounded by polyester fiber-fill and covered by a nearly air-tight polyester film. The freezing/melting features were still evident in the temperature data, but had been reduced significantly. Next a small bag of desiccant was added to the polyester fiber-fill and dry Freon<sup>TM</sup> gas was sprayed into the fiber-fill so as to displace any moisture. The freezing/melting features were completely eliminated with this last step. Temperature data was taken with this insulation arrangement and the results are displayed in Fig. 15. The quality of this cold heat exchanger temperature data is good enough for accurate exponential curve fitting, if some of the data near the refrigerator's initial turn-on and turn-off points are excluded.



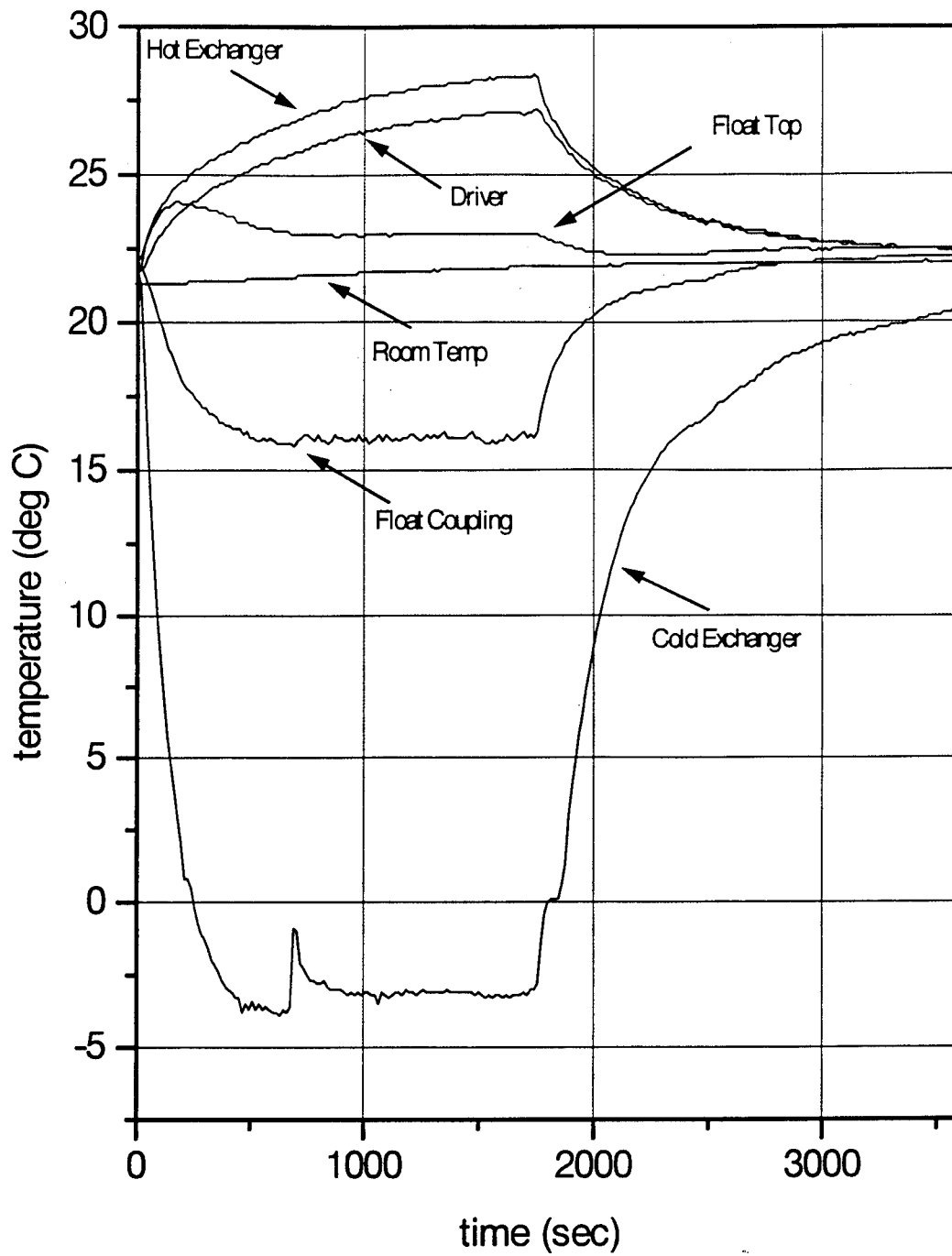


Figure 14. Time Dependent Refrigerator Performance, Uninsulated

The following is a brief discussion of the other 5 temperature curves in Fig. 15. The flat curve at  $21.5^{\circ}\text{C}$  is simply a room temperature value. The curve representing the float coupling (the fitting joining the small diameter tube to the float) cools down to about  $12.5^{\circ}\text{C}$  before the refrigeration is stopped. With the insulation, the thermal coupling between the cold heat exchanger is strong enough to cause a pronounced cooling in spite of the acoustic dissipation in that region and the heat leak from the outside.

The temperature at the top of the float starts by climbing above room temperature by a few degrees, then turns around and cools to about  $0.5^{\circ}\text{C}$  below room temperature before the refrigeration is stopped. This is significant, because it means that as temperatures equilibrate following cool down, all of the acoustic dissipation in the resonator above the cold heat exchanger is eventually transported to the cold heat exchanger as heat. By contrast, in Fig. 14 the float top temperatures always stay above room temperature, which means some of the acoustic dissipation is conducted directly to the room as heat.

The driver and hot heat exchanger temperatures both get hotter than room temperature by several degrees. Interestingly, the hot heat exchanger gets slightly hotter than the driver.

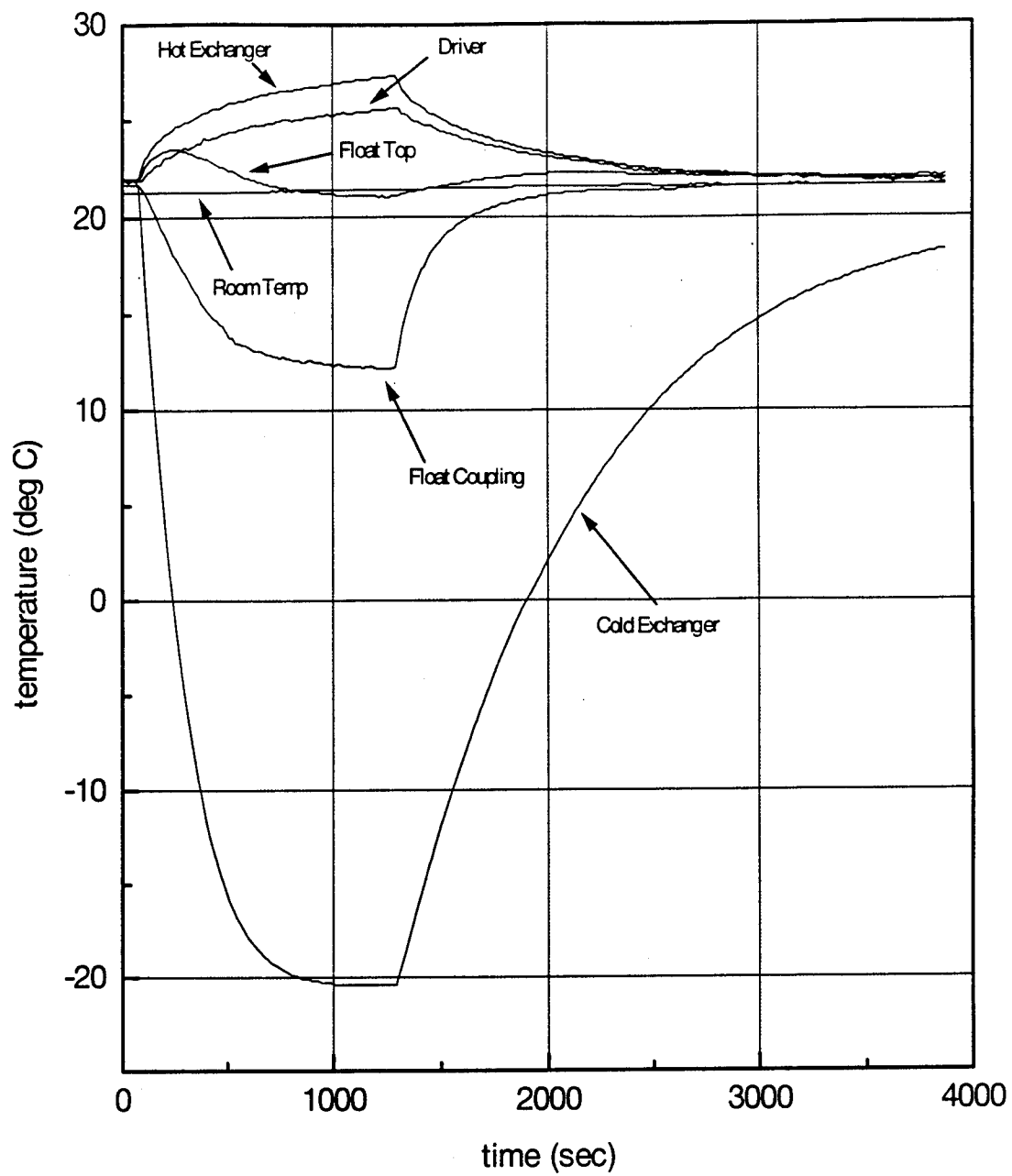


Figure 15. Time Dependent Refrigerator Performance, Insulated

### 3. Cold Heat Capacity Gives Heat Power Information.

The rate at which the temperature of the cold heat exchanger changes in the previous plots depends on the total heat power entering or leaving the exchanger  $Q_{TOT}$ , and it depends on the total heat capacity  $C_p$  of all of the parts in intimate thermal contact with the exchanger. The time rate of change of the cold exchanger temperature multiplied by the total heat capacity should give the total heat power entering the cold exchanger portion, hence;

$$Q_{TOT} = \frac{dT_C}{dt} C_p . \quad 5)$$

First we will determine the total heat capacity of all of the parts in intimate thermal contact with the cold exchanger. These parts are: the copper reducer, cold heat exchanger, stainless steel stack flange and stainless steel screws. Total volume calculated for the copper was  $1.536 \text{ in}^3$ . Total volume of stainless steel was  $0.340 \text{ in}^3$ . Since the specific heat  $c_p$  is usually specified per-unit-mass, the specific heat per unit volume is given by  $\rho c_p$ , where  $\rho$  is the mass density of the material.

The values for these particular constants were taken from [Ref. 14]. The heat capacities of the copper and stainless steel portions are given in Eqs. 6 & 7, with sum or total given in Eq. 8.

$$C_p(Cu) = V_{Cu} \times \rho_{Cu} \times c_p \quad 6)$$

$$C_p(Cu) = \left[ \frac{1.536 \text{ in}^3 \text{ cm}^3}{6.102 \times 10^{-2} \text{ in}^3} \right] \left[ \frac{8.96 \text{ g}}{\text{cm}^3} \right] \left[ \frac{0.380 \text{ J}}{\text{g} - \text{K}} \right]$$

$$= \underline{85.75 \text{ J/K}}$$

$$C_p(SS) = V_{ss} \times \rho_{ss} \times C_p \quad 7)$$

$$C_p(SS) = \left[ \frac{0.3398 \text{ in}^3 \text{ cm}^3}{6.102 \times 10^{-2} \text{ in}^3} \right] \left[ \frac{7.9 \text{ g}}{\text{cm}^3} \right] \left[ \frac{0.500 \text{ J}}{\text{g} - \text{K}} \right]$$

$$= \underline{21.99 \text{ J/K}}$$

$$C_p = C_p(Cu) + C_p(SS) \quad 8)$$

$$= \underline{107.74 \text{ J/K}}$$

If we assume that portions of the time dependent temperature data in Fig. 15, can be fitted to an exponential curve, then the resulting formula for the cold exchanger temperature would be,

$$T_C(t) = T_0 + A_0 e^{-(t-t_0)/\tau} \quad 9)$$

The time derivative of the cold temperature used in Eq. 9 is then given by,

$$\frac{dT_C}{dt} = \frac{-A_0}{\tau} e^{-(t-t_0)/\tau} = \frac{-1}{\tau} (\Delta T(t)), \quad 10)$$

where  $\Delta T(t) = T_C(t) - T_0$ . Here  $T_0$  is a limiting temperature value that would be achieved in steady state equilibrium at long time values. This limiting value is near room temperature for the warm-up data, but it is the limiting coldest temperature for the cool-down data.

Combining Eqs. 5 and 10 we have,

$$Q_{TOT} = \frac{-C_p}{\tau} \Delta T(t) = K \Delta T(t), \quad (11)$$

or 
$$K \equiv \frac{-C_p}{\tau}, \quad (12)$$

where K is defined to be a total conductance for the cold exchanger portion.

In the case of the warm-up portion of the cold exchanger temperature data in Fig. 15, where the refrigerator is turned off,  $K_{HL}$  would represent the total "heat leak" to the warmer room and driver. In the case of the cool-down data, a total conductance  $K_{EC}$  can also be calculated which corresponds to an "excess cooling" power given by the difference between the total active cooling power of the refrigerator and the heat leak power from room temperature. The total conductances are,

$$K_{HL} = \frac{-C_p}{\tau_{wu}}, \quad (13)$$

and 
$$K_{EC} = \frac{-C_p}{\tau_{cd}}, \quad (14)$$

where  $\tau_{wu}$  and  $\tau_{cd}$  are the warm-up and cool-down time constants respectively. These time constants are determined by fitting the exponential formula of Eq. 10 to the experimental data. The following are numerical values for the above:  $\tau_{wu} = 984.2$  sec,  $\tau_{cd} = 221.9$  sec,  $K_{HL} = 0.109 \text{ W}/^\circ\text{C}$ , and  $K_{EC} = 0.486 \text{ W}/^\circ\text{C}$ .

$$Q_{TC} = Q_{EC} + Q_{HL} = K_{EC} \Delta T_{cd} + K_{HL} \Delta T_{wu} \quad (15)$$

Equation 15 represents the total cooling power developed from the operation of the refrigerator. For example, with a  $\Delta T = 24.1^\circ \text{C}$ , the total cooling power for the demonstration refrigerator is 14.32 watts. A plot of these results will be given in section D, where this method will be compared with a different method.

#### **4. Driver and Hot Heat Exchanger Temp with Fast and Slow Fans.**

Earlier in Chapter II, calculations were conducted to optimize the proper fan size to meet the cooling requirements of the acoustic driver with the cowling installed. Based on that preliminary calculation, two fans were purchased with equal outer dimensions. The volume flow rate capacities, however, were not the same. The first fan, which will be referred to as the slow fan, has a 34 cfm flow rate. The second fan or fast fan has a 105 cfm flow rate. Both fans, through actual testing, proved they could provide sufficient cooling to the driver. In the end, the fast fan was chosen. The following reasons were the deciding factors. During all test runs the slow fan maintained the driver at about 30° to 31° C at the refrigerator's coldest operating temperature. The fast fan maintained the driver temperature at approximately 26° to 26.5° C. This represented about a 4° to 4.5° C improvement over the slow fan. The added cooling capability was felt to be an important asset, especially when the unit may be required to operate in a warm, humid, and/or drafty lecture auditorium.

Another consideration was the noise factor during actual operation. The slow fan was designed to be very quiet, and added little noise to the refrigerator operation. The fast fan was considerably noisier, generating a moderate amount of broadband or "white" noise. In spite of this fact, the fast fan may be the best choice with respect to overall noise. Although slightly noisier, the fast fan also provided some masking of the high pitch sound produced by the acoustic driver. Total sound produced by the acoustic driver and fan was still low enough to allow for normal speaking during lecture demonstrations.

An observation made from the temperature data showed the driver to be about 3° to 4° C cooler compared to the hot heat exchanger using either fan. Better thermal coupling between the aluminum flange containing the hot heat exchanger and the aluminum driver housing would provide some extra cooling of the hot heat exchanger. This could produce slightly cooler cold temperatures. Also, the hot exchanger flange could be re-made with more fins with more surface area for heat dissipation. This issue was not answered in this study, but could be implemented as an improvement.

## D. STEADY STATE COOLING POWER WITH ELECTRIC HEAT LOADS

### 1. Thermal and Acoustic Power Measurement Procedures.

A second method of measuring the refrigerator's performance was also used. This procedure included the use of an electrically powered heater strip applied directly to the cold heat exchanger body. It provided a constant heat source or heat load for the cooling power of the refrigerator.

Using a regulated dc power supply,<sup>(7)</sup> a specific current or voltage could be applied to obtain a given heat load for the refrigerator. The heater strip had a measured resistance of 46.3 ohms. Electric power inputs were set via the dc power supply<sup>(7)</sup> at values between 1 and 12 watts of power.

The cold heat exchanger was insulated as before and the operating frequency was set at 655 Hz. The peak acoustic pressure  $p_o$  was maintained at 5% of the mean resonator pressure  $p_m$ , or  $p_o/p_m = 5\%$ . The microphone sensitivity was equal to 3.05 V/bar; a value taken from previous research done by Adeff [Ref. 15]. The 5% pressure ratio, therefore, corresponded to a microphone voltage of 0.677 V rms as indicated on a digital multimeter.<sup>(6)</sup> This microphone voltage was regulated manually with the gain knob on the power amplifier<sup>(1)</sup> that was connected to the acoustic driver. Typically, a driver input current of about 1.58 A rms was required to produce this microphone output voltage.

During these heat load and temperature measurements, both the electric power delivered to the driver and the acoustic power delivered to the resonator were also measured. The impedance analyzer<sup>(2)</sup> was used as a gain-phase meter for the electric power supplied to the acoustic driver and for the acoustic signals coming from the two transducers inside the driver. Two pairs of cables were alternately connected to the single pair of inputs on the signal analyzer. These measurements, along with appropriate calibration constants for the acoustic transducers can be used in the following power equations.



$$\text{Electric power:} \quad P_{elect} = V_{ac} \times I_{ac} \cos\theta \quad 16)$$

$$\text{Acoustic power:} \quad W = P \times U \cos \phi \quad 17)$$

The electric power equation should be obvious, and the acoustic power equation is analogous, where  $P$  refers to the rms acoustic pressure amplitude at the driver piston,  $U$  refers to the rms volume velocity delivered by the driver piston, and  $\phi$  is the phase between  $P$  and  $U$ . With these measured quantities, the efficiency of the driver and refrigerator can be determined. This is covered in subsection 3 below.

The detailed measurement procedure began with starting the refrigerator and maintaining an amplitude of  $p_o/p_m = 5\%$ . With the electric heater disconnected, the refrigerator was allowed to cool down and equilibrate at its coldest temperature. Then data was taken of the temperatures, the acoustic power, and the electric driver power. The heater was then turned on and various heat loads were applied to the cold heat exchanger. The applied heat loads varied from 1 watt to 12 watts in one and two watt increments. At each heater value, the temperatures were allowed to equilibrate and they were recorded. Also, the heater power, acoustic power, and electric driver power was recorded.

## **2. Comparing Steady State and Time Dependent Cooling Power Data.**

A plot comparing steady state excess cooling power versus time dependent excess cooling power is displayed in Fig. 16. The slopes of the two sets of data output are nearly the same. The difference between the two linear plots could be caused by differences in the quality of the thermal insulation. Also note that we were not measuring acoustic pressure amplitude during the time dependent temperature measurements. Also, the drive current of 1.85 A rms was somewhat higher than the typical drive current for the steady state measurements. We expect that the steady state measurements are much more accurate. However, the heat leak power is always determined from the time dependent warm-up data.

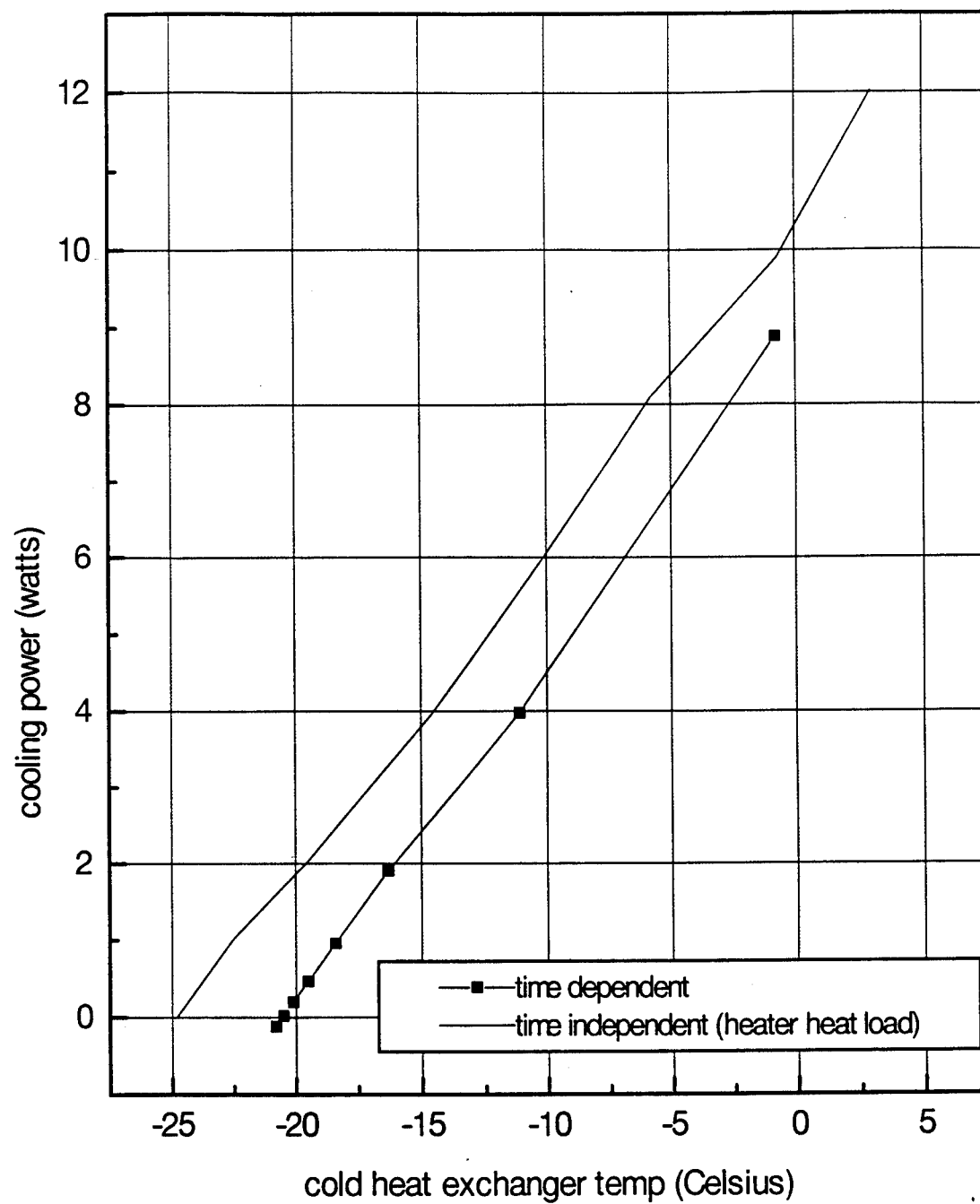
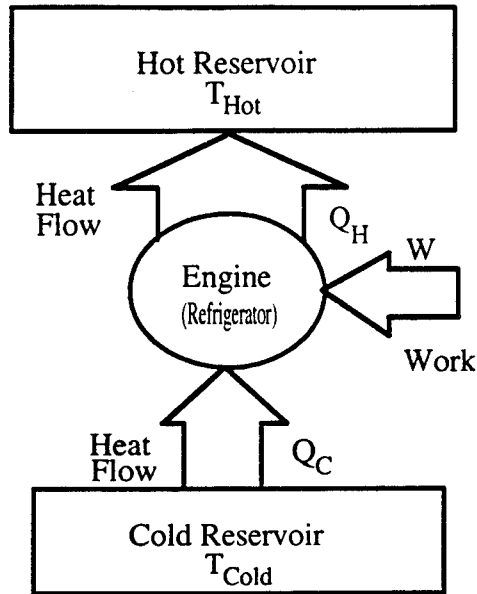


Figure 16. Steady State and Time Dependent Cooling Power Data

### 3. Computing Coefficient of Performance and Efficiencies.

We begin with a discussion of the basic quantities involved in the operation of a heat pump. From this, we can define the dimensionless quantity, coefficient of performance, or COP and we can calculate the COP for a perfect or Carnot engine. The diagram below shows a schematic view of an operating heat pump.



G. S. Swift describes this process.

....work is absorbed by the engine, resulting in the pumping action of heat from low temperature to high temperature [Ref. 4].

The coefficient of performance is defined to be the ratio of the two powers that are most relevant to performance of a refrigerator.

$$COP \equiv \frac{Q_C}{W} \quad 18)$$

The cooling power  $Q_C$  is the whole purpose of the engine, and the input power  $W$ , is energy usage required by the engine to achieve this purpose.

The 1st and 2nd laws of thermodynamics govern this operation and they are respectively:

$$Q_H = W + Q_c \quad (19)$$

$$\frac{Q_c}{T_c} \leq \frac{Q_H}{T_H} \quad (20)$$

The variable  $Q_c$  is the heat flow lifted from the cold thermal reservoir,  $Q_H$  is the heat flow dumped to the hot thermal reservoir,  $W$  is the work input required by the engine,  $T_c$  &  $T_H$  are the temperatures of the cold and hot reservoirs (the bottom and top of the diagram respectively). Equation 19 is simply conservation of energy and Eq. 20 states that the total entropy of the process either remains constant or increases. If equations 19 & 20 are combined, the following equation is obtained.

$$COP = \frac{Q_c}{W} \leq \frac{T_c}{T_H - T_c} \quad (21)$$

Note that the right hand side of the above inequality is an upper limit on the COP, and can be much greater than unity for a small temperature span refrigerator. For this reason, the term COP is used rather than “efficiency” since the latter term always refers to a quantity that has an upper limit of unity.

The acoustic COP as well as coefficient of performance relative to that of a Carnot engine ( $COP_R$ ) were calculated for the demonstration refrigerator as part of the performance evaluation. The following formulas were used:

$$COP_{TC} = \frac{Q_{TC}}{W} \quad (22)$$

$$COPR_{TC} = \frac{COP_{TC}}{COP_{Carnot}} = COP_{TC} \left[ \frac{T_H - T_c}{T_c} \right] \quad (23)$$

Here  $W$  is the acoustic power.  $T_H$  and  $T_c$  are the temperatures of the hot heat exchanger and the cold heat exchanger respectively, and  $Q_{TC}$  is the total cooling power as defined in Eq. 15. Note that Eqs. 22 and 23 roughly describe the intrinsic acoustic to

thermal performance of the thermoacoustic stack and not the overall performance of the refrigerator as a useful product. A more precise determination of intrinsic stack performance would require measurement of the temperatures inside the resonator, which we were not able to do. A plot of COP and temperature span for the steady state measurements is shown in Fig. 17.

Demo Refrig.: 90 psia He; po/pm = 5%; 665 Hz; 9/7/94

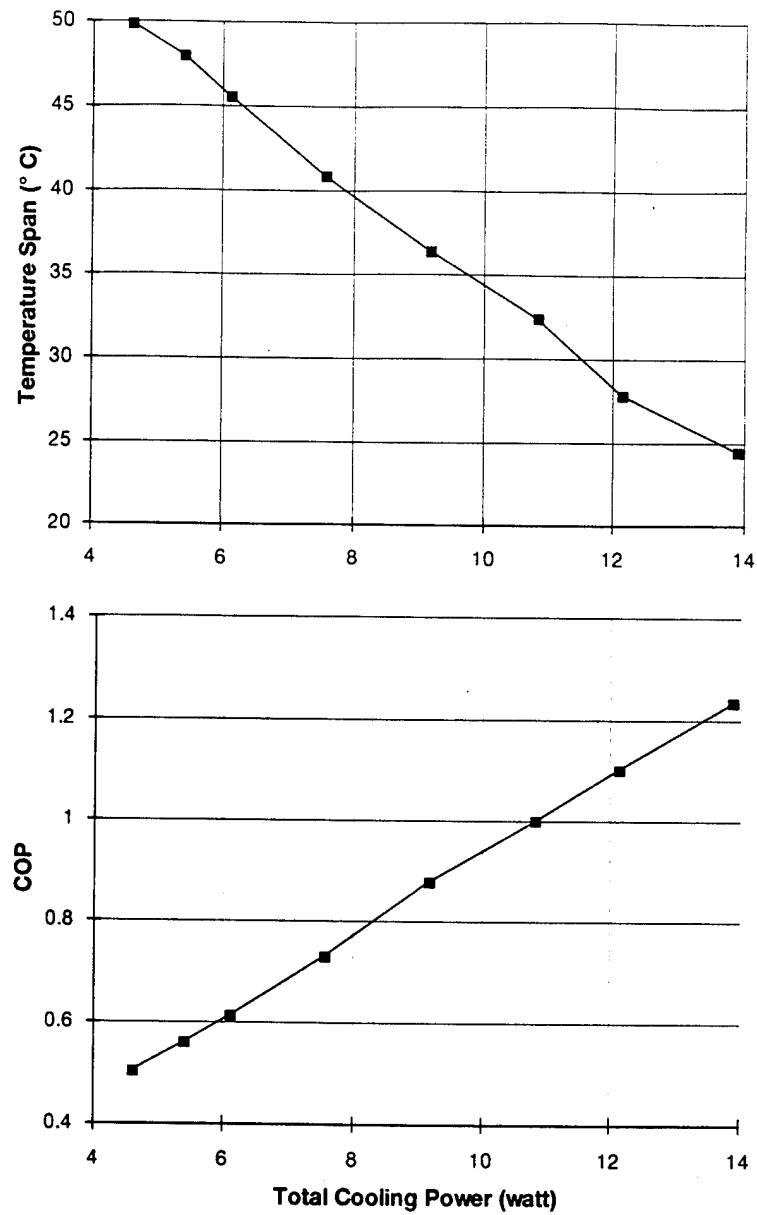


Figure 17. Plots of Total Cooling Power versus Temperature Span and COP

Additional calculations included the computation of the acoustic driver efficiency  $\eta$  and coefficient of performance  $COP_{elect}$  based on the electric power supplying the acoustic driver. The equations are given below:

$$\eta = \frac{W}{P_{elect}} \quad 24)$$

$$COP_{elect} = \eta COP_{TC} = \frac{Q_{TC}}{P_{elect}} \quad 25)$$

The results for all of the above quantities are shown in the table below.

Qc(Excess)	Qc(Total)	T Span	COP(TC)	COPR(TC)	COP(Elec)
watt	watt	deg C			
0.00	4.61	49.9	0.51	0.101	0.17
1.02	5.40	48.0	0.56	0.107	0.19
2.02	6.11	45.6	0.61	0.110	0.21
3.95	7.55	40.9	0.73	0.116	0.26
6.00	9.16	36.4	0.88	0.121	0.31
8.09	10.82	32.4	1.00	0.121	0.36
9.90	12.13	27.9	1.10	0.113	0.39
12.02	13.88	24.5	1.23	0.110	0.44

**Table 1 Performance results for steady state measurements.**

The driver efficiency  $\eta$  was generally about 35%.

As an example, at 8.09 watts of electric heater heat load the total heat load (with heat leak) was 10.82 watts, and the demonstration refrigerator produced the following results: Temperature span = 32.4° C,  $COP_{TC} = 1.00$ ,  $COPR_{TC} = 0.121$ , and  $COP_{elect} = 0.36$ . This roughly corresponds to the performance values calculated for the Brooks thesis. The Brooks predictions for a total cooling power of 11.1 watts at  $p_o/p_m = 5\%$  were: Temperature span = 35° C,  $COP_{TC} = 1.15$ ,  $COPR_{TC} = 0.15$ . Note that this last group of numbers are slightly different than those in the Brooks thesis, since the acoustic resonator losses are now being entirely included as a heat load on the cold heat exchanger. This change is based on the results of section C-2 where we learned that the float temperature cools below room temperature with an insulated resonator.

Also, we are including the temperature defects in the internal heat exchangers as estimated by Lt. Brooks. And finally, some of the remaining discrepancy can be explained by the extra temperature defect between the internal hot heat exchanger and the aluminum fins where the thermocouple was attached. We do not have a measurement for this temperature defect, although it is probably on the order of two degrees.





## **IV. PACKAGING**

### **A. COMPACT/EFFICIENT ELECTRIC POWER AMPLIFIER**

#### **1. Basic Circuit.**

In order to meet the original objectives, a simple, compact, and efficient power amplifier circuit was designed. The design had to be compact in order to fit within a hard shelled carrying case, along with the refrigerator, and provide sufficient power. Efficiency is important because the heat dissipation of most amplifiers require large and heavy heat sinks. The basic requirements were 2 A rms output at 650 Hz with a 9 ohm load, for 36 watts of power output.

The input square wave from a switching circuit is filtered by the tank circuit in order to produce a nearly sinusoidal output wave at about 650 Hz for the acoustic driver. Utilizing circuit analysis software [Ref. 16], Dr. Hofler was able to evaluate a L-R-C tank circuit for use with the demonstration refrigerator. The analysis software was useful in determining the circuit values that produced an acceptable level of output distortion and usable frequency bandwidth, with the smallest value of inductance. The inductor is the largest and most expensive part of the amplifier; smaller inductance values are also smaller in size. An inductance value of 5 mH and a capacitance value of 12  $\mu\text{F}$  was chosen.

#### **2. Inductor used with Circuit.**

The inductor core size now had to be determined. Ferrite inductor cores were chosen with a split "E" geometry, a core air gap, and a plastic coil bobbin. The air gap provides a stable inductance value with respect to differences in inductor current and temperature. Also, air gapped inductors are generally more efficient and less likely to saturate because the air gap dominates the core characteristics independent of the magnetic material properties and losses.

Two different core sizes were purchased. Equation 23 was utilized to obtain the number of windings on the core based on the core constant  $L_0$ .

$$N = \sqrt{\frac{L}{L_0}} \times 1000 \quad 23)$$

Here  $L$  is the 5 mH derived from the computer program and  $L_0$  depends on the inductor core size chosen. The copper coils are hand wound on the plastic bobbin. The two core pieces are inserted into the bobbin and bolted together.

The first inductor built utilized a 250 mH core with 20 gauge wire. The best inductor performance achieved with the test circuit; however, was with a 90 mH core using 18 gauge magnet wire. This inductor required 235 turns. The actual inductance measured via the impedance analyzer<sup>2</sup> was 5.10 mH with a total resistance of 0.5 ohms at 650 Hz.

### 3. Square Wave Switching Circuit.

The circuit that generates the 650 Hz frequency and drives the LRC tank circuit is shown in Fig. 17. A standard CD4047 CMOS timer integrated circuit, U1, generates the 650 Hz square wave. It is a low power device and conveniently provides both non-inverted and inverted outputs at pin 10 and 11. Roughly speaking, the 4047 outputs are buffered by the bipolar transistor network, Q1-Q5, which then drives the gates of the power MOSFETs Q6 and Q7. These two power MOSFETs form the push-pull stage that powers the L-R-C tank circuit with a square wave.

The function of the bipolar drive stage deserves some discussion since it does more than buffer the outputs of U1. Note that MOSFETs Q6 and Q7 alternately turn on and off. Only one can be in the on-state at any given instant. Simultaneous conduction of both Q6 and Q7, even for a tiny fraction of the cycle, will destroy both. For this reason, some "dead time" is required, where both devices are briefly off at the same time during the transitions of the square wave. This "dead time" is provided by resistor R9 which delays the transition of Q6 to the on-state, and by resistor R8 which delays the transition

of Q7 to the on-state. There is an RC time-constant associated with both R8 and R9 because of the gate capacitance of the power MOSFETs.

The resulting “dead time” can cause short inductive spikes from the tank inductor L1. These high frequency spikes are reduced or “snubbed” by R10 and C2. Components R10 and C2 have little effect on the efficiency because the frequencies of the 650 Hz square wave are much lower.

Also, the part of the bipolar transistor network containing devices Q1, Q4, and Q5 provides a voltage shifting function as well. The output from pin 11 of the timer device U1, can only swing between 0 and 12 volts, but the gate of MOSFET Q6 must swing between 32 and 42 volts.

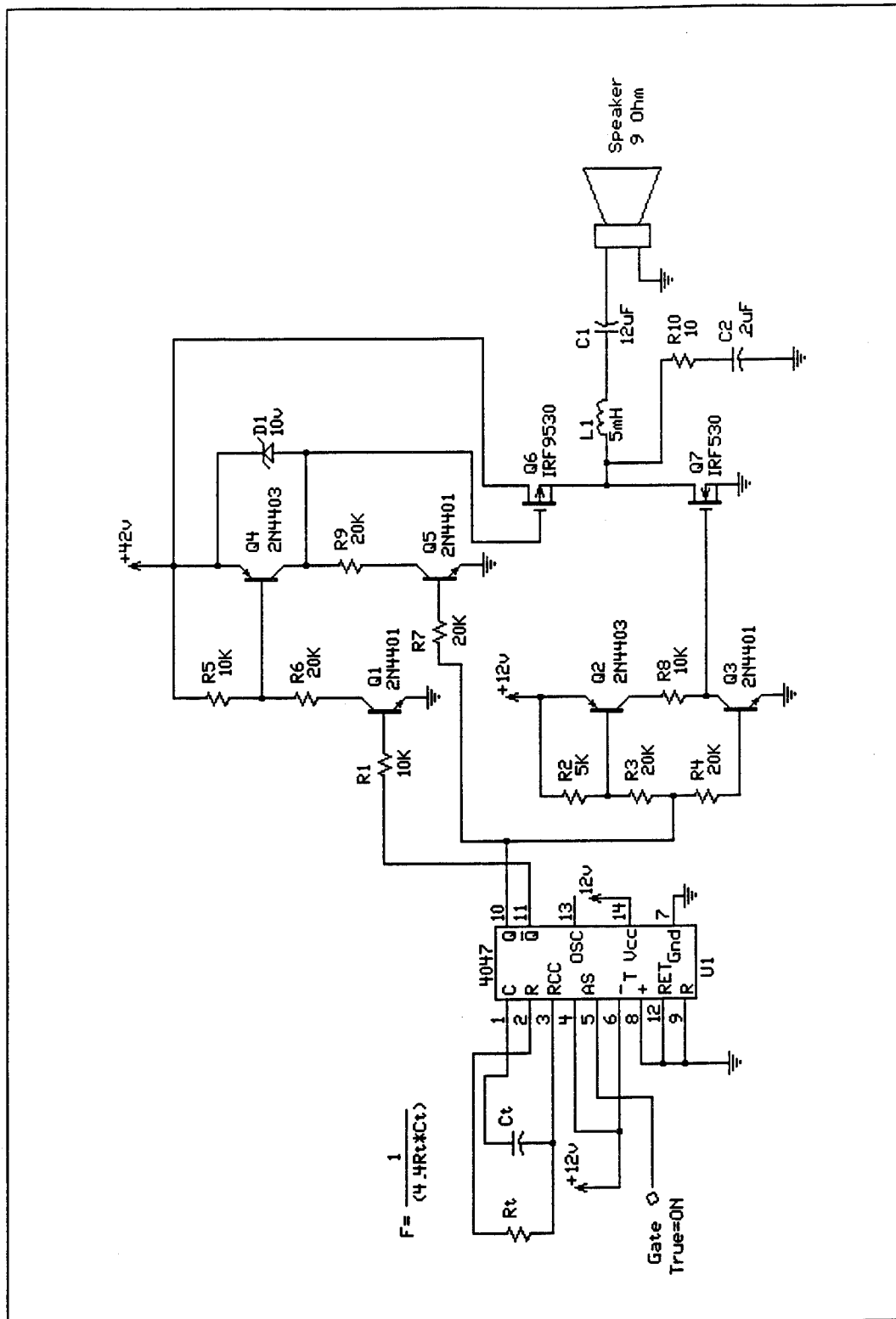


Figure 18. Acoustic Driver Circuit Schematic

#### **4. Efficiency with Load Resistor.**

Because of time limitations, the above circuit was not tested with the demonstration refrigerator, but it was briefly tested with a load resistor connected to the tank circuit, at an output current level of about 1 A rms. Current and voltage readings were taken from the meters on a dc power supply<sup>(7)</sup> used to power the circuit and the true-rms voltage on the load resistor was measured. The ratio of ac output power to dc input power was determined to be about 90%. This should be considered a preliminary measurement only. However, this appears to be promising, since typical ac power amplifiers are only about 50% efficient.

#### **B. ANCILLARY EQUIPMENT**

The remaining sub-systems of the demonstration refrigerator were the carrying case, two 115 V<sub>ac</sub> thermocouple thermometers (LED displays with a +/- 0.1 degree of resolution), the clear plastic air deflector plate, and the aluminum resonator protective cover. The carrying case and LED thermocouple thermometers are self explanatory. The clear plastic air deflector plate mentioned in Chapter III, part C, section 2 was manufactured locally. See the appendix for a diagram. The reason for the air deflector plate was to prevent the air flow from impinging on the cold heat exchanger on its way to the air intake at the hot heat exchanger. The clear Lucite deflector plate reduced the heat load on the cold heat exchanger without hiding the hot heat exchanger parts below it from view. Finally, the aluminum protective cover for the resonator is shown in the appendix as well. The protective cover was manufactured for added protection of the resonator while the demonstration refrigerator is in transit.



## **V. CONCLUSION**

### **A. SUCCESSFUL DEMONSTRATION**

The major goal of building a working thermoacoustic refrigerator has been accomplished. The thermoacoustic demonstration apparatus achieves the objectives. The copper reducer and cold heat exchanger will produce frost under the work input of the acoustic driver. The apparatus provides an excellent lecture tool for dramatically displaying the capabilities of thermoacoustic heat transfer.

The efficiency was not quite as good as predicted by Lt. Brooks [Ref. 7]. Lt. Brooks optimized the demonstration refrigerator via a computer model and achieved a 20.8% COPR. This value; however, was based on internal stack temperatures and a partial heat load from the resonator dissipation. The COPR subsequently calculated via laboratory measurements was found to be 12.1%. See Table 1. This value was based on external temperatures.

The difference in COPR values can be attributed to the extra heat load from resonator dissipation and temperature defects in the heat exchange paths. Some of the those temperature defects are the following: temperature difference between the stack ends and the internal heat exchangers; the defect within the internal heat exchangers; the interface between aluminum finned flange element and hot heat exchanger (coupled via heat sink grease), and finally the defect along the aluminum heat sink fins. The thermocouple was attached to the outer end of an aluminum fin.

The relative efficiency (COPR), although lower than predicted, still meets the objectives of the demonstration apparatus.

### **B. POWER DENSITY IMPROVEMENT**

The cooling power density of this design could be increased by perhaps a factor of 10 without increasing the overall size of the package substantially. The tube diameters of the resonator could be increased by 50% to 100% without affecting the length of the



resonator. Also, both the relative acoustic pressure  $p_o/p_m$  and the mean pressure  $p_m$ , could be increased by 50%. The primary problem is in providing enough acoustic drive power.

A solution to the drive power problem would be to utilize a different driver altogether. Another driver was designed in a thesis project by Lt. Monahan [Ref. 17]. It describes a more powerful and efficient driver design which could be substituted for the Mode/Adeff driver. This particular driver could be driven at approximately 60 watts of acoustic power and it has a predicted electric to acoustic efficiency of 80%. However, 60 watts of acoustic power is not quite enough unless the intrinsic thermoacoustic efficiency is improved.

### **C. THERMOACOUSTIC EFFICIENCY IMPROVEMENT**

Improvement of thermoacoustic efficiency is much more difficult. Another means of efficiency improvement may be the use of inert gas mixtures within the resonator. These mixtures lower the Prandtl number of the gas and reduce the dissipation caused by viscosity. This is perhaps the most promising means for improvement. None of these recommendations were explored. They could serve as basis for further research into a practical design for a commercial refrigeration unit using thermoacoustic principles.

### **D. PROBLEMS AND SUGGESTIONS**

In Chap. 3, resonant frequencies were measured for the insulated and uninsulated resonator. Variations in the resonant frequency were expected and measured depending on the distribution of cold temperatures in the resonator. However, differences were also measured when both insulated and uninsulated resonators were uniformly at room temperature. Near the end of the work on this project we discovered that the helium gas in the resonator was slowly becoming slightly contaminated. We confirmed this conclusion by refilling and purging the system with helium. The resulting resonant frequencies were a few Hz higher than the highest previous measurements, and 20 or 25 Hz higher than just before the refilling process.

This had never been encountered in previous thermoacoustic refrigerators, so we had not anticipated this to be a problem here. Apparently, the resonator had not been thoroughly purged initially which perhaps accounted for a 10 Hz difference. Also, this refrigerator incorporated a new driver and had been used for a period of several months without being refilled. Usually, a month is the typical operational time period for previous refrigerator experiments. While every attempt is made to ensure that the resonator is clean before final assembly, the driver is a different matter. The driver contains a number of materials such as epoxies, adhesives, and plastics that could outgas and contaminate the helium with substantially heavier organic based gases. These heavier gases could make their way into the resonator via the capillary leak between the driver and resonator.

In the future, more care needs to be taken with respect to the initial gas purging process and perhaps subsequent purging on a periodic basis.



## **APPENDIX. CONSTRUCTION DRAWINGS**

This section contains construction drawings for the shroud for air cooling, the air deflector plate, and the aluminum protective resonator cover for the portable demonstration refrigerator.

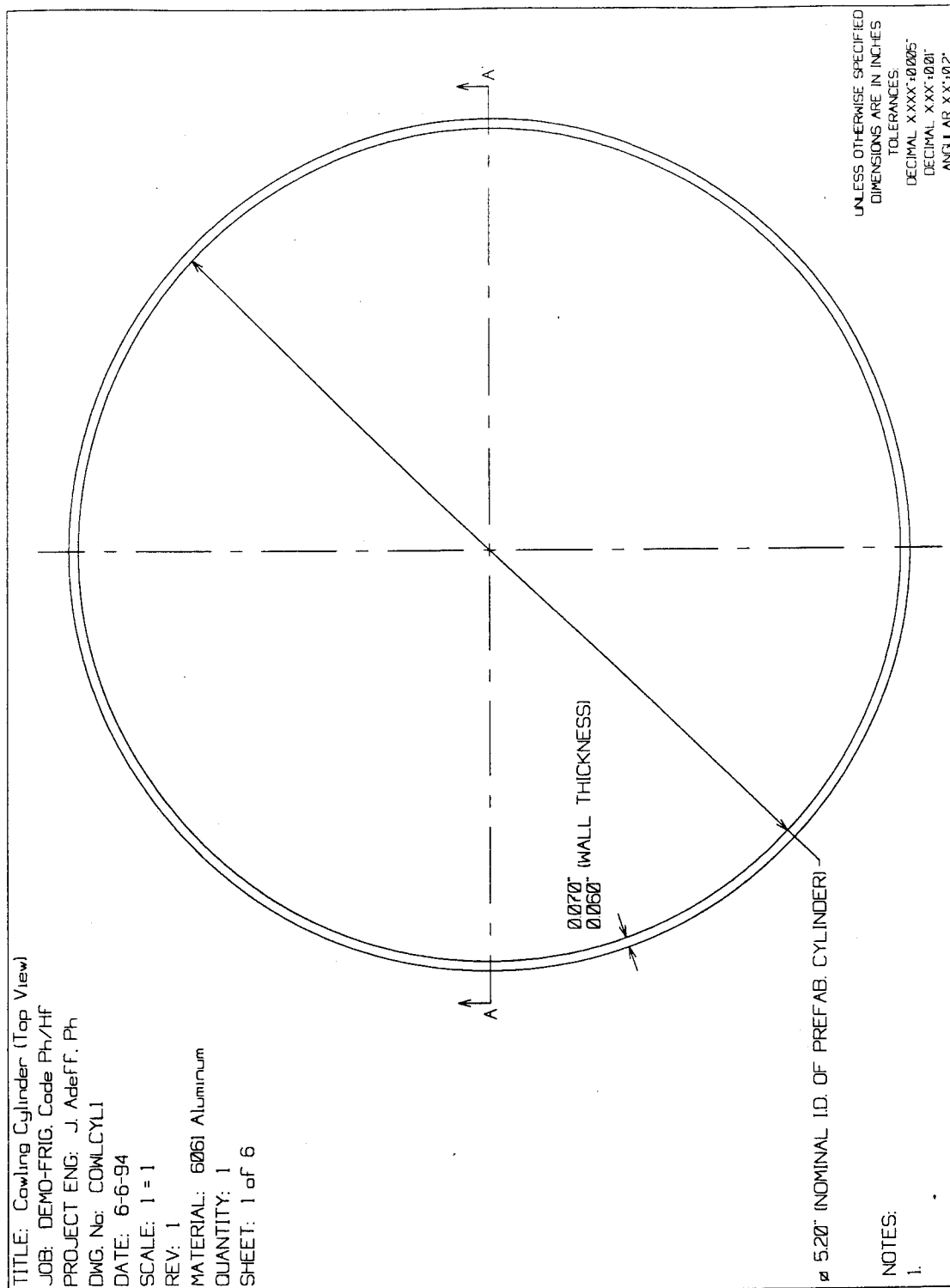


Figure 19. Cowling Cylinder (drawing #1)

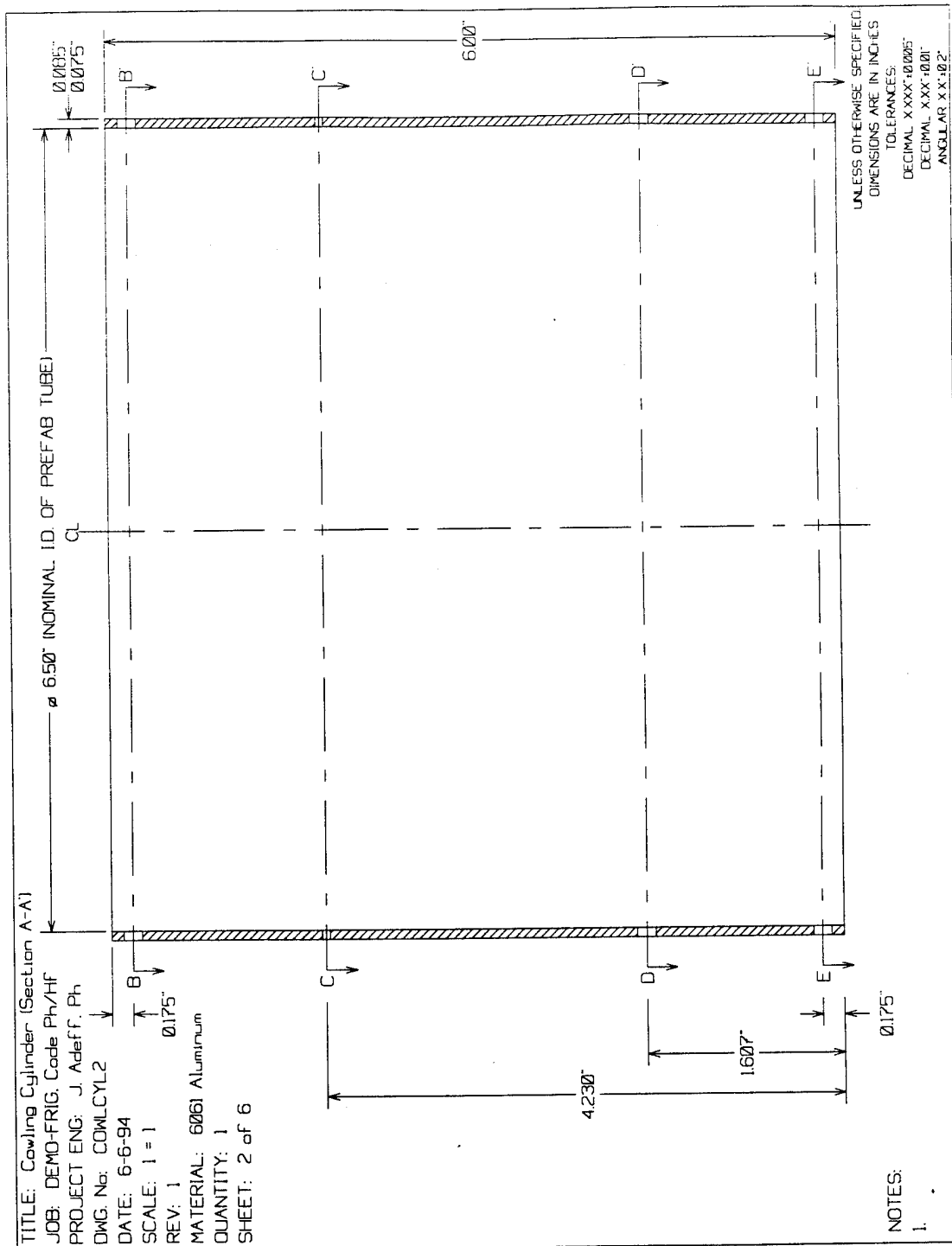


Figure 20. Cowling Cylinder (drawing #2)

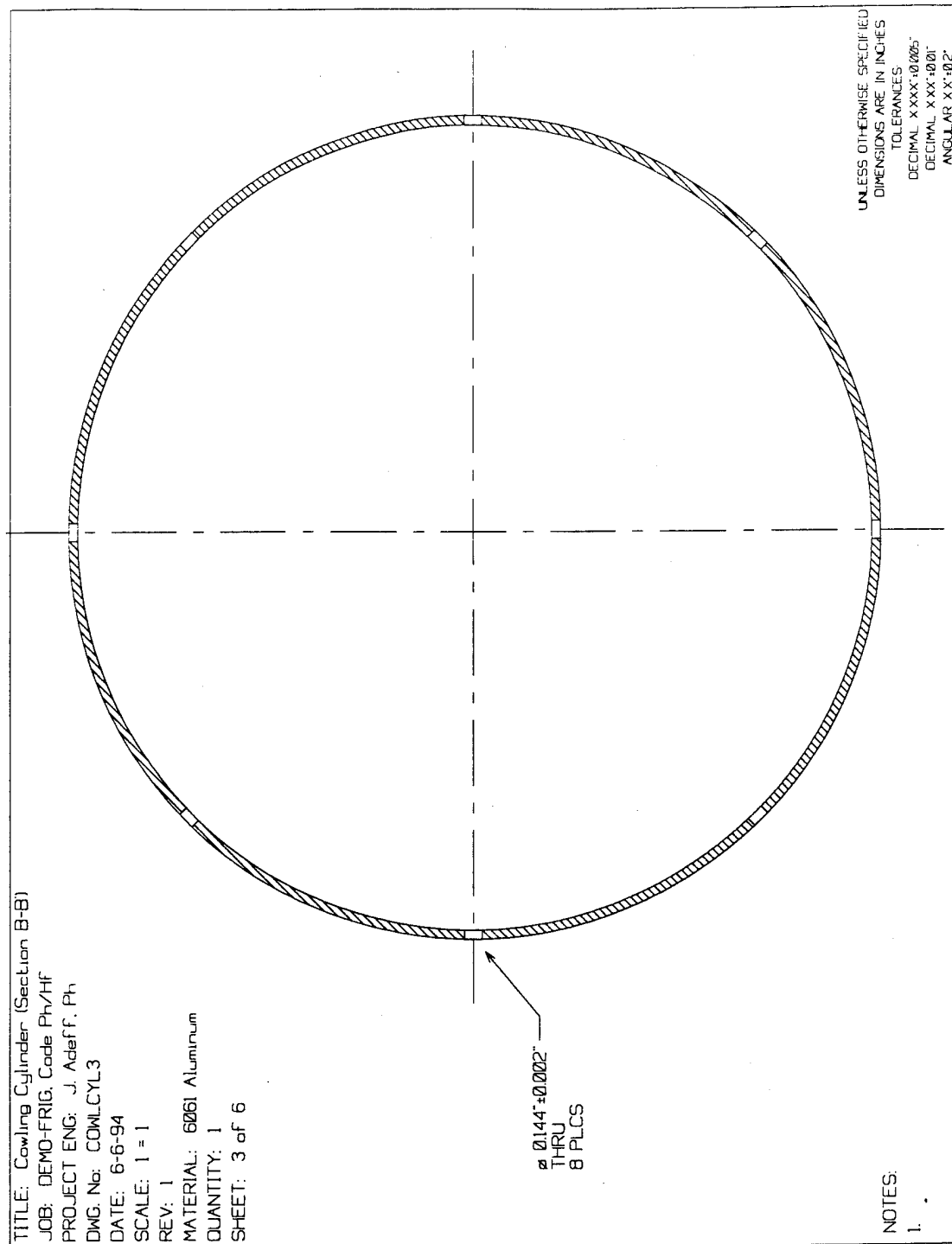


Figure 21. Cowling Cylinder (drawing #3)

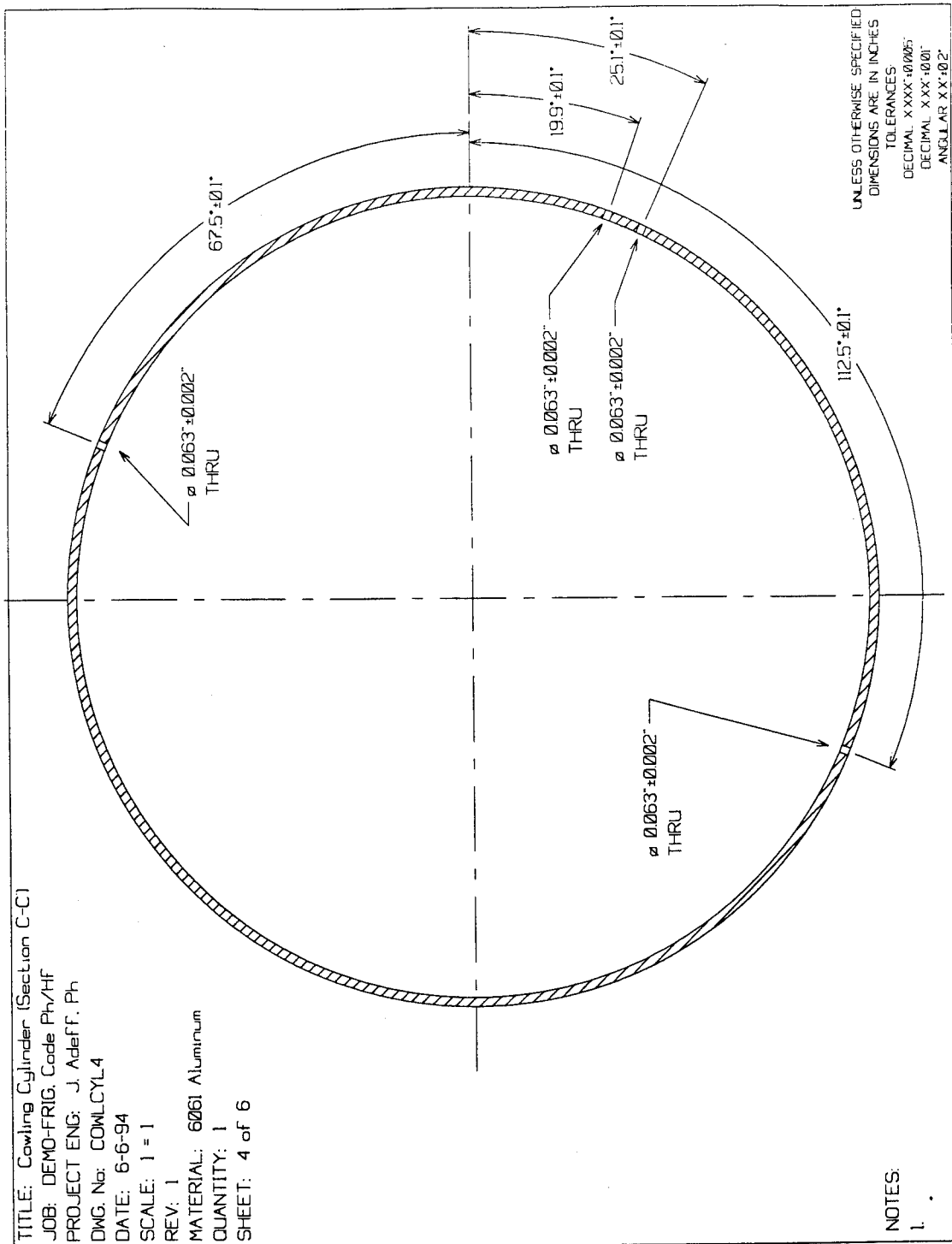


Figure 22. Cowling Cylinder (drawing #4)



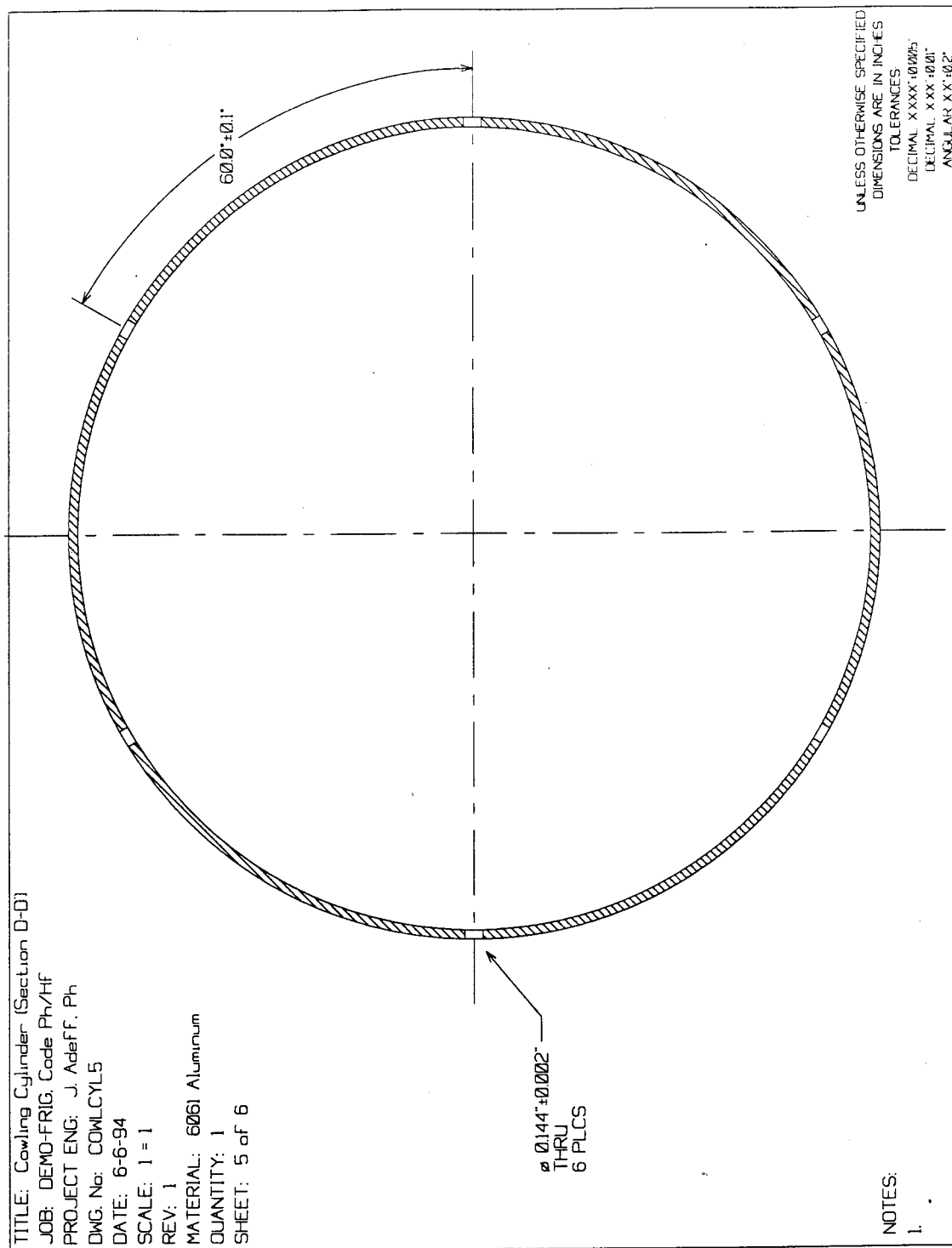


Figure 23. Cowling Cylinder (drawing #5)

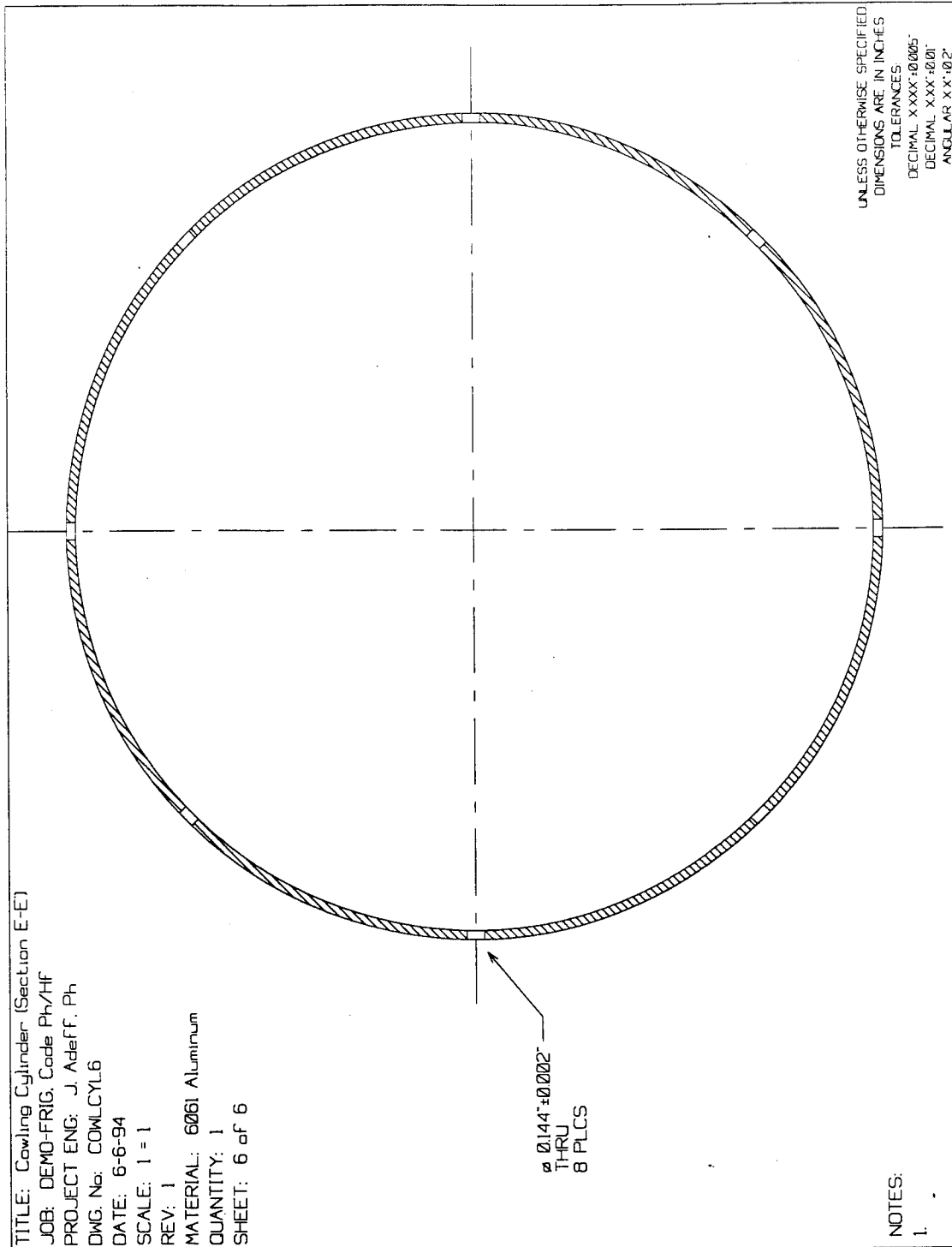


Figure 24. Cowling Cylinder (drawing #6)

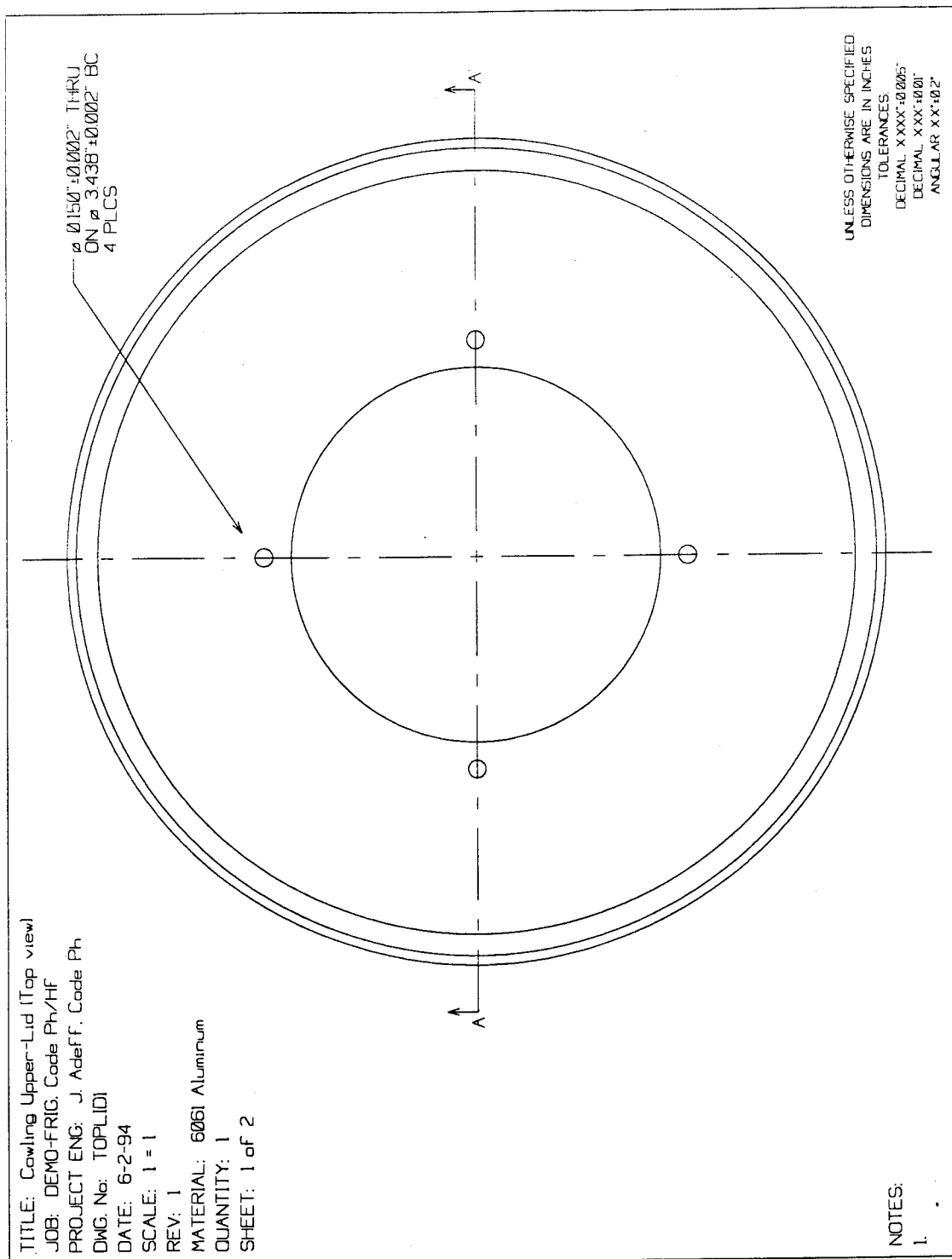


Figure 25. Cowling Lid (drawing # 1)

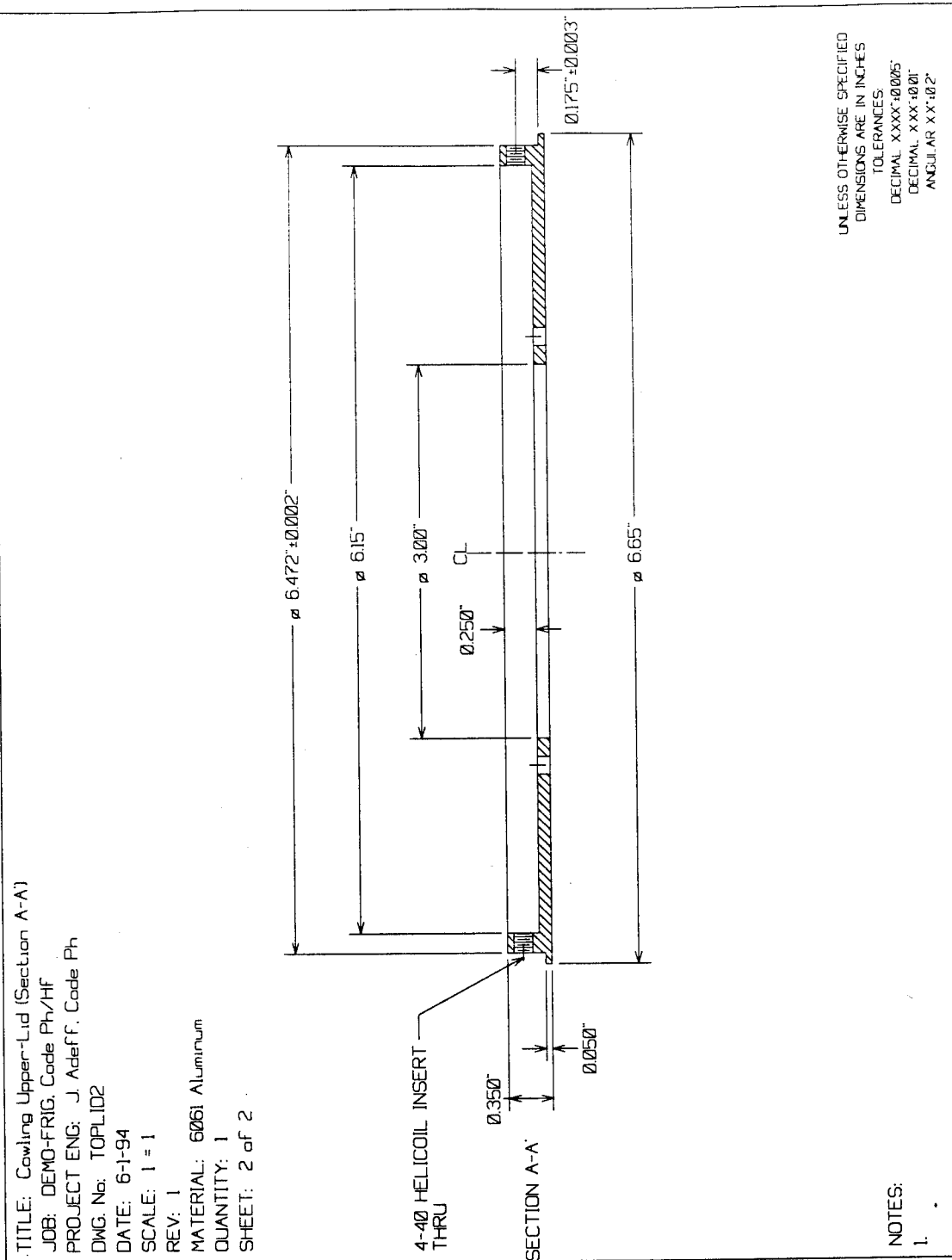
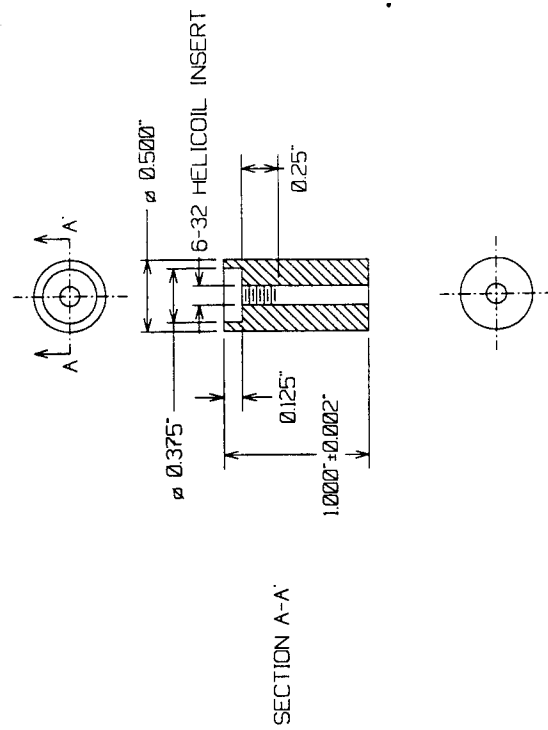


Figure 26. Cowling Lid (drawing # 2)

TITLE: Legs  
 JOB: DEMO-FRIG. Code Ph/Hf  
 PROJECT ENG: J. Adef F. Code Ph  
 DWG. No: DEMOLEGS  
 DATE: 6-27-94  
 SCALE: 1 = 1  
 REV: 1  
 MATERIAL: Delrin  
 QUANTITY: 4

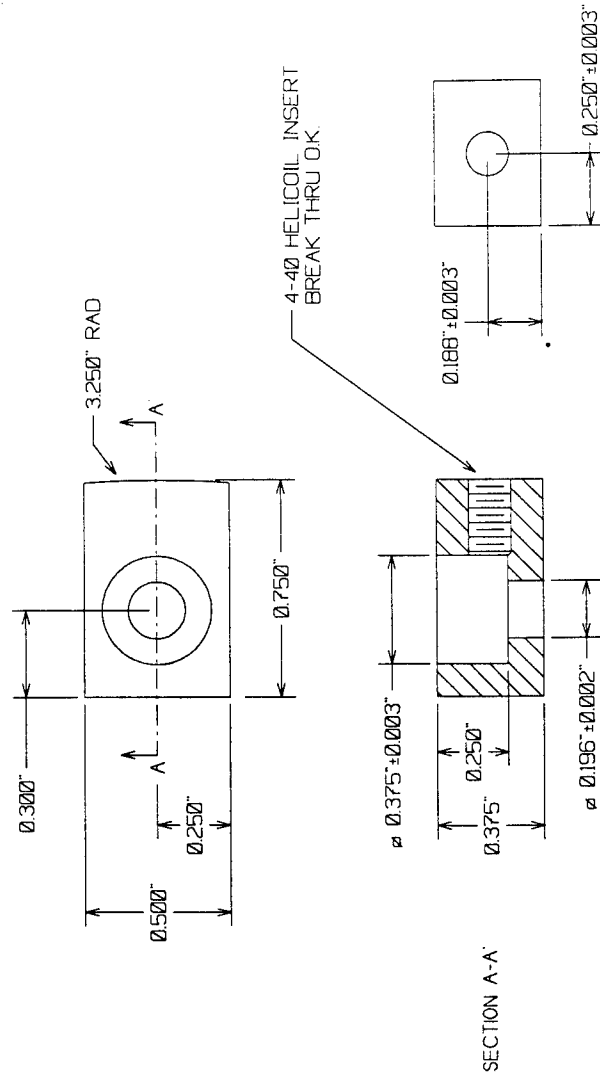


UNLESS OTHERWISE SPECIFIED  
 DIMENSIONS ARE IN INCHES  
 TOLERANCES:  
 DECIMAL XXXX ± 0.0005  
 DECIMAL XX ± 0.01  
 ANGULAR XX ± 0.2°

NOTES:  
 1.

Figure 27. Cowling Legs

TITLE: Cowling Bracket  
 JOB: DEMO-FRIG, Code Ph/Hf  
 PROJECT ENG: J. Adeff, Code Ph  
 DWG. No: COWLBRKT  
 DATE: 6-6-94  
 SCALE: 1 = 2  
 REV: 1  
 MATERIAL: 6061 Aluminum  
 QUANTITY: 6



UNLESS OTHERWISE SPECIFIED  
 DIMENSIONS ARE IN INCHES  
 TOLERANCES:  
 DECIMAL XXXX: ±0.005"  
 DECIMAL XXX: ±0.01"  
 ANGULAR X°: ±0.2°

NOTES:  
 1. Drawing shown twice actual-size. Do not scale.

Figure 28. Cowling Bracket

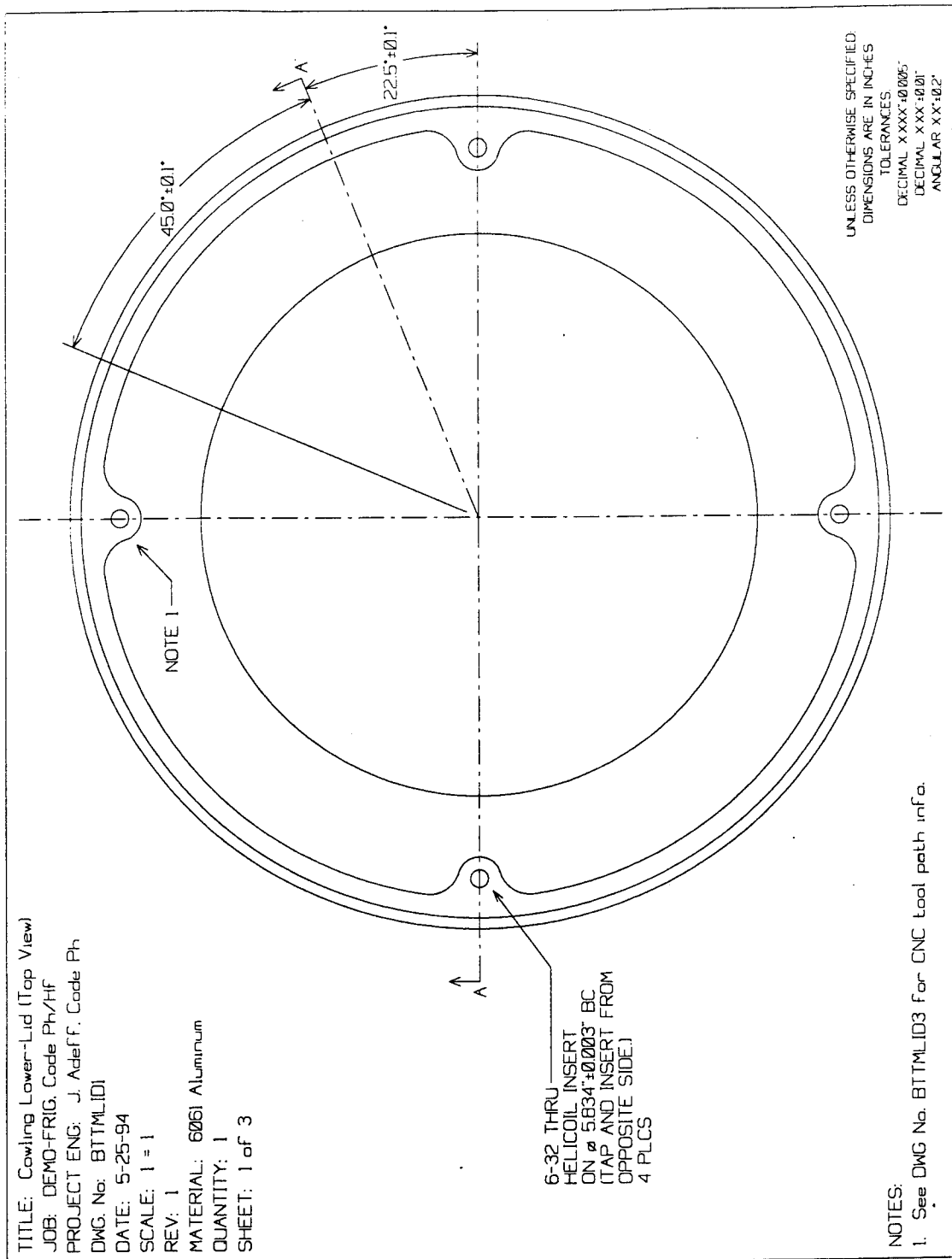
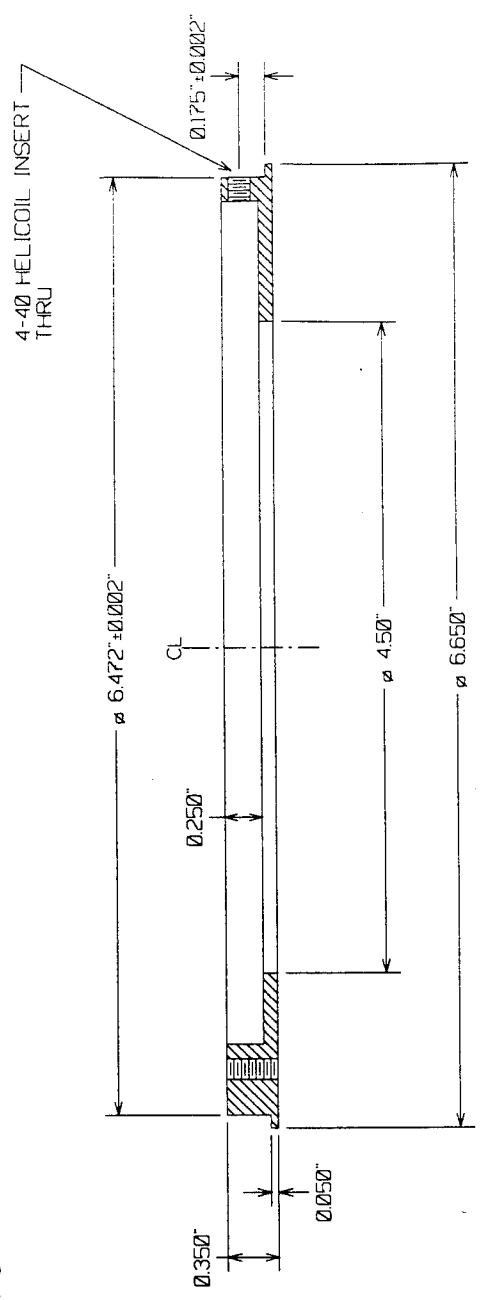


Figure 29. Cowling Base (drawing # 1)

TITLE: Cowling Bottom-lid (Section)  
 JOB: DEMO-FRIG. Code Ph/HF  
 PROJECT ENG: J. Adeff. Code Ph  
 DWG. No: BTMLID2  
 DATE: 6-1-94  
 SCALE: 1 = 1  
 REV: 1  
 MATERIAL: 6061 Aluminum  
 QUANTITY: 1  
 SHEET: 2 of 3



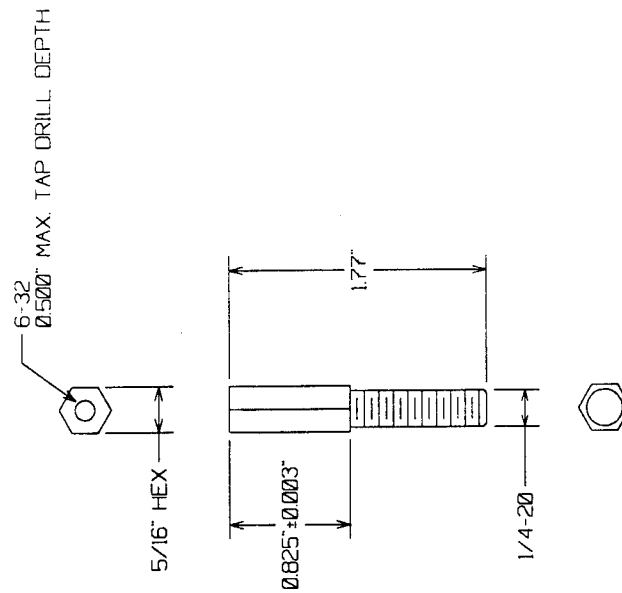
UNLESS OTHERWISE SPECIFIED  
 DIMENSIONS ARE IN INCHES  
 TOLERANCES  
 DECIMAL XXX ± 0.005  
 DECIMAL XX ± 0.01  
 ANGULAR XX ± 0.2

NOTES:  
 1.

Figure 30. Cowling Base (drawing # 2)



TITLE: 1/4-20 to 6-32 Standoff-Adeptar  
 JOB: DEMO-FRIG. Code Ph/Hf  
 PROJECT ENG: J. Adeff. Code Ph  
 DWG. No: STANDOFF  
 DATE: 6-7-94  
 SCALE: 1 = 1  
 REV: 1  
 MATERIAL: Stainless Steel (any 300 series)  
 QUANTITY: 4



UNLESS OTHERWISE SPECIFIED:  
 DIMENSIONS ARE IN INCHES  
 TOLERANCES:  
 DECIMAL XXXX±0.005  
 DECIMAL XXX±0.001  
 ANGULAR XX°±0.2°

NOTES:  
 1.

Figure 31. Resonator Flange Standoff

QUANTITY: 1

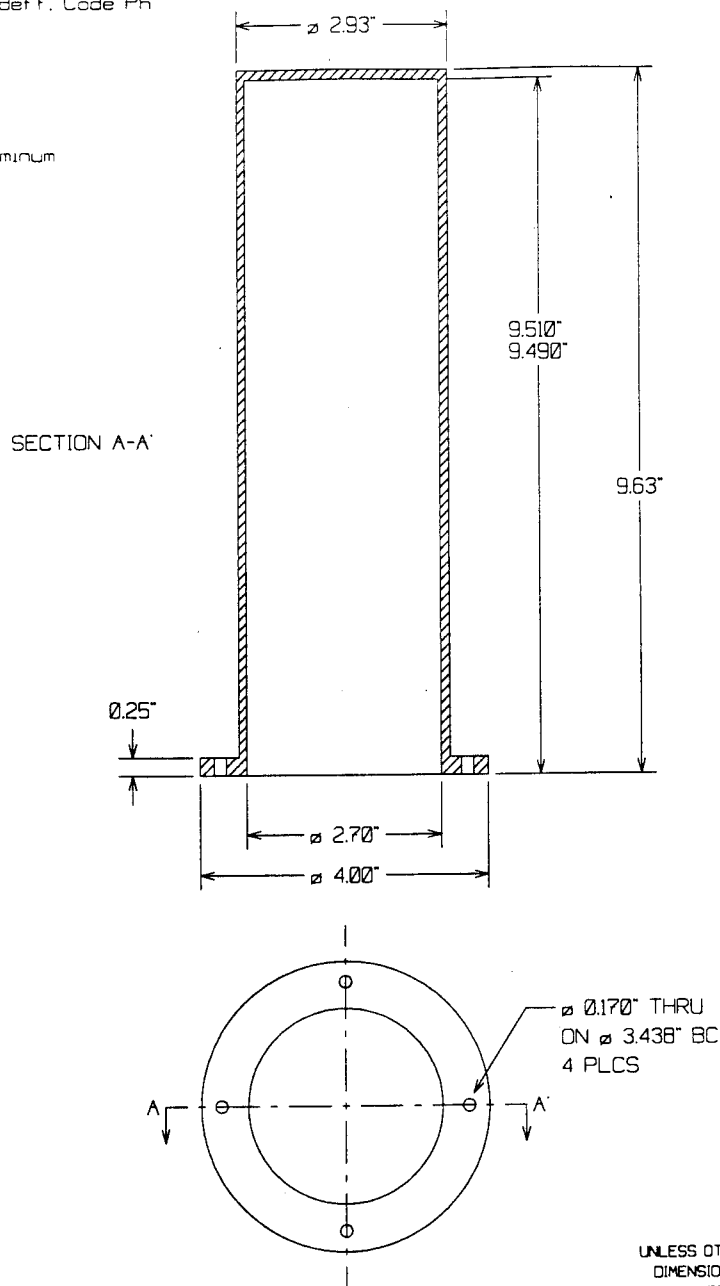


1000

—

### Figure 32. Valve Stem Extension

TITLE: Demo-Frig. Resonator Shield  
 JOB: TAR3, Code Ph/HF  
 PROJECT ENG: J. Adeff, Code Ph  
 DWG. No: RESSHLD  
 DATE: 11-9-94  
 SCALE: 1 = 2  
 REV: 1  
 MATERIAL: 6061 Aluminum  
 QUANTITY: 1



NOTES:

1. Objects shown half life-size. Do not scale.

UNLESS OTHERWISE SPECIFIED:  
 DIMENSIONS ARE IN INCHES  
 TOLERANCES:  
 DECIMAL XXXX $\pm$ 0.005"  
 DECIMAL XXX $\pm$ 0.01"  
 ANGULAR XX $\pm$ 0.2°

Figure 33. Resonator Shield

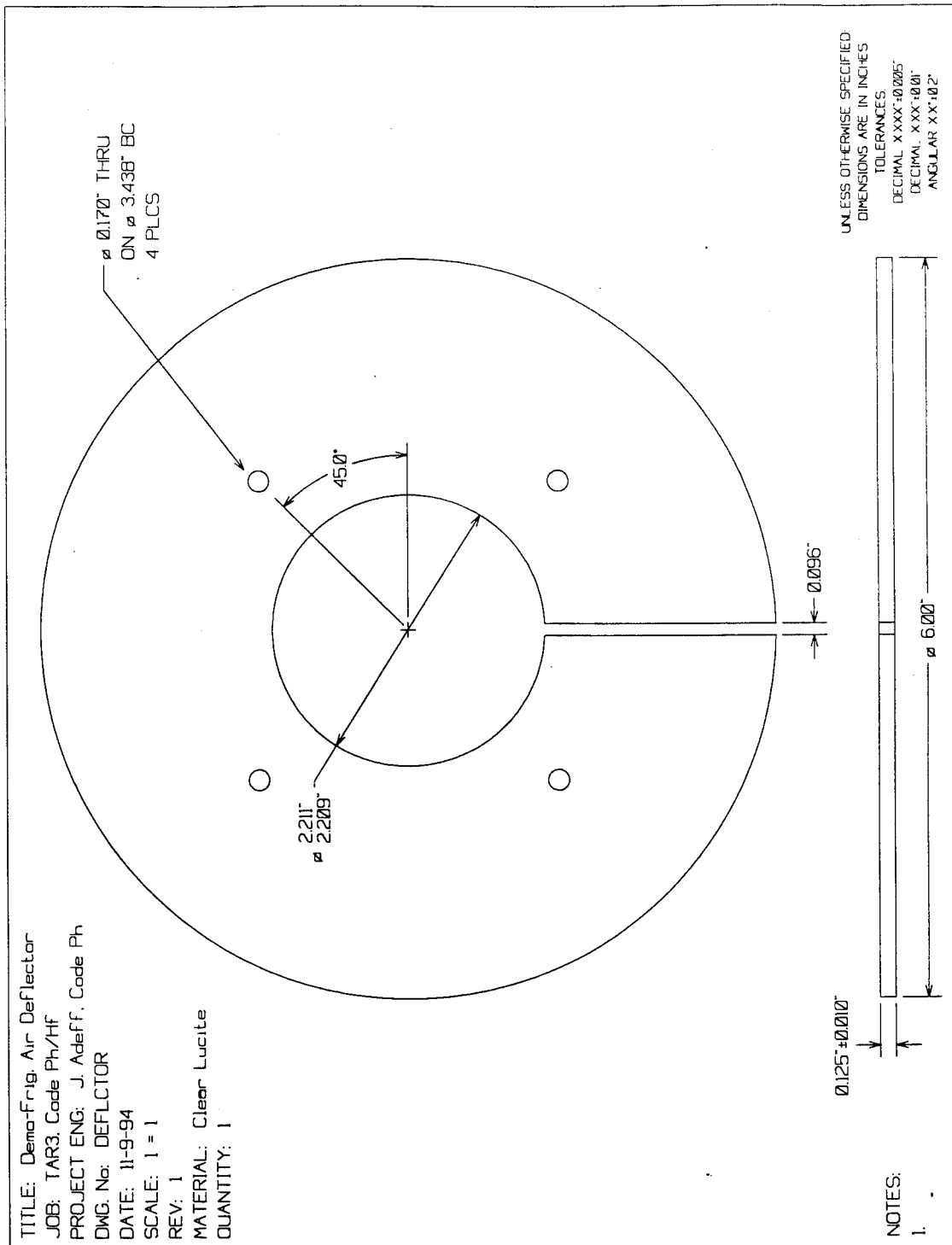


Figure 34. Air Deflector

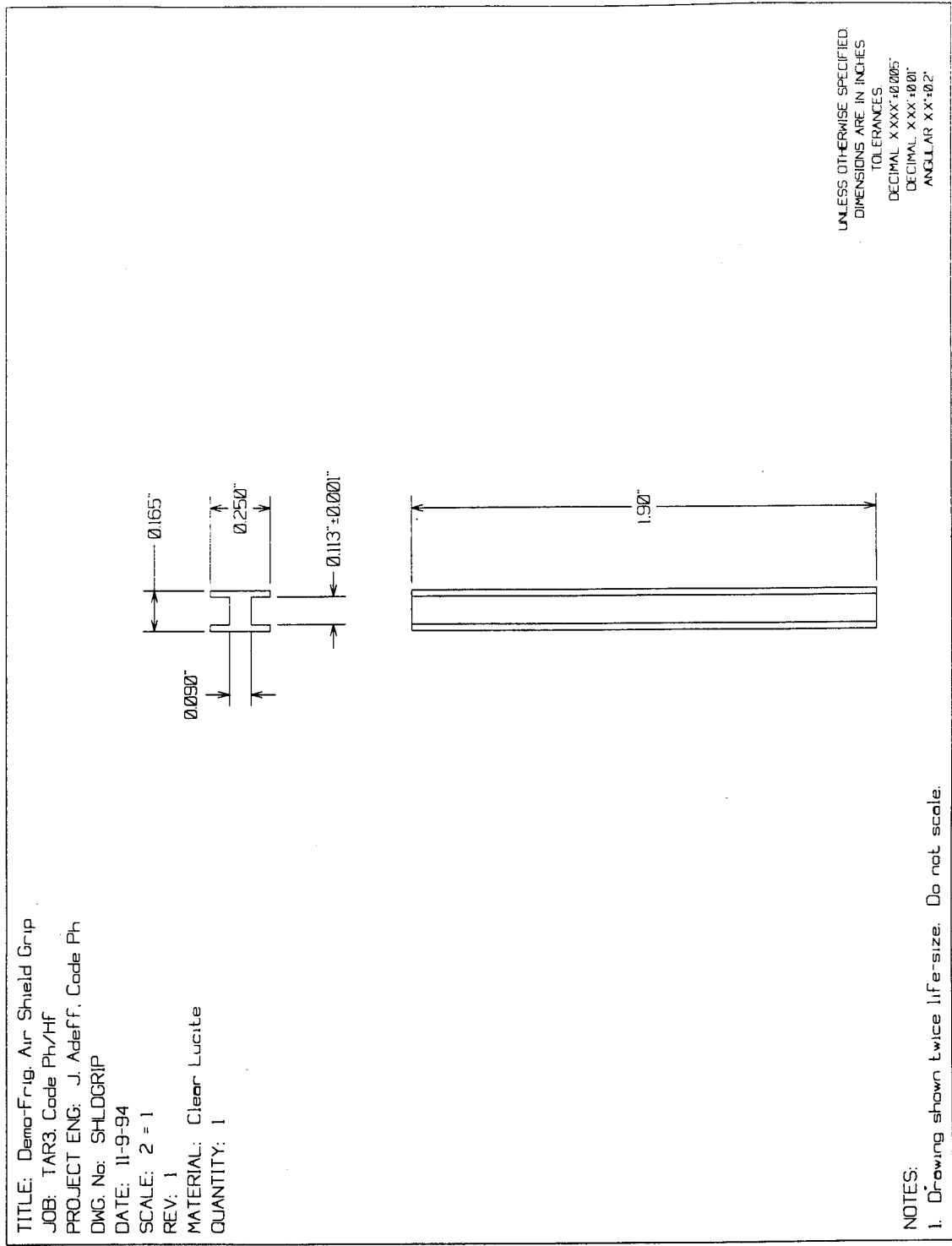


Figure 35. Air Shield Grip

## LIST OF REFERENCES

1. Rott, N., "Thermoacoustics," *Advanced Applied Mechanics*, v. 20, p.135, 1980.
2. Wheatley, J. C., Hofler, T. J., Swift, G. W., and Migliori, A., "An Intrinsically Irreversible Thermosacoustic Heat Engine," *Journal of the Acoustic Society of America*, v. 74, p.153, 1983.
3. Hofler, T. J., *Thermoacoustic Refrigerator Design and Performance*, Ph.D. Dissertation, University of California, San Diego, California, 1986.
4. Swift, G. W., "Thermoacoustic Engines," *Journal of the Acoustic Society of America*, v. 84, p. 1145, 1988.
5. Adeff, J. A., *Measurement of the Space Thermoacoustic Refrigerator Performance*, Master's Thesis, Naval Postgraduate School, Monterey, California, September 1990.
6. Atchley, Anthony A., and Hofler, Thomas J., "Thermoacoustic Heat Pumps," *Journal of the Acoustical Society of America* v. 87, Sup. 1, S32 (A), 1990.
7. Brooks, B. R., *Construction of a Thermoacoustic Refrigerator Demonstration Apparatus*, Naval Postgraduate School, Monterey, California, March 1994.
8. Mode, K. S., *Development of a Higher Amplitude Thermoacoustic Driver Having a Relatively Wide Frequency Bandwidth*, Naval Postgraduate School, Monterey, California, March 1994.
9. Landau, L. D. and Lifshitz, E. M., *Fluid Mechanics*, v. 6, pp. 49 & 56, Copyright 1959, reprinted 1975, Library of Congress Catalog Card Number: 59-10525, ISBN 0-08-09104-0.
10. COMAIR-ROTRON Corporation, 2675 Customhouse Court, San Ysidro, CA 92173.
11. Hofler, T. J., "Accurate Acoustic Power Measurements with a High Intensity Driver," *Journal of the Acoustic Society of America*, v. 83, p. 777, 1988.
12. Wheatley, J. C., "The Natural Heat Engine," *Los Alamos Science*, number 14, pp. 2-17, Fall 1986.
13. Adeff, J. A., Electric to Acoustic Efficiencies of a Driver connected to a Test Resonator, Unpublished Data, Naval Postgraduate School, Monterey, California, March 1994.

14. Boyer, H. E. and Gall, T. L., Editors, *Metals Handbook*, American Society for Metals (Desk Edition) pp. 1-49,67, Copyright 1985, reprinted 1992, Library of Congress Catalog Card Number: 84-71465, ISBN: 0-87170-188-X.
15. Adeff, J. A., Microphone Sensitivity calibration conducted at Naval Postgraduate School, Monterey, California, June 1994.
16. Micro-Cap III, Electronic Circuit Analysis Program, Version 3, Published by Spectrum Software 1021 S. Wolfe Road, Sunnyvale, California 94086.
17. Monahan, D. A., *Design Improvements for a High Efficiency Thermoacoustic Driver*, Naval Postgraduate School, Monterey, California, March 1994.

## INITIAL DISTRIBUTION LIST

	# Copies
1. Defense Technical Information Center ..... Cameron Station Alexandria, VA 22304-6145	2
2. Library, Code 52 ..... Naval Postgraduate School Monterey, CA 93943-5101	2
3. Professor T. Hofler, Code PH/HF ..... Naval Postgraduate School Monterey, CA 93943-5100	5
4. Professor Anthony A. Atchley, Code PH/AY ..... Naval Postgraduate School Monterey, CA 93943-5100	1
5. Jay Adeff, Code PH/AF ..... Naval Postgraduate School Monterey, CA 93943-5100	1
6. LT Todd J. Berhow, USN ..... 32349 Oxford Mill Road Cannon Falls, MN 55009	2